

Probing evolutionary mechanisms in galaxy clusters: neutral atomic hydrogen in Abell 1367

T. C. Scott,¹★ H. Bravo-Alfaro,² E. Brinks,¹ C. A. Caretta,² L. Cortese,³ A. Boselli⁴
M. J. Hardcastle,¹ J. H. Croston¹ and I. Plachu²

¹Centre for Astrophysics Research, University of Hertfordshire, College Lane, Hatfield AL10 9AB

²Departamento de Astronomía, Universidad de Guanajuato. Apdo, Postal 144, Guanajuato 36000, Mexico

³School of Physics and Astronomy, Cardiff University, Cardiff CF24 3AA

⁴Laboratoire d'Astrophysique de Marseille, OAMP, Université Aix-Marseille 8 CNRS, 38 Rue Frédéric Joliot-Curie, 13388 Marseille, France

Accepted 2009 December 10. Received 2009 December 10; in original form 2008 December 24

ABSTRACT

We present Very Large Array H I imaging data for a field in the NW of the galaxy cluster Abell 1367 ($z = 0.02$) in an attempt to probe the effect environment has on the interstellar medium of late-type spiral galaxies. Several galaxies, like CGCG 097–087, show pronounced tails and asymmetries, and seven out of 10 show significant, several kpc offsets between the H I centroid and the optical. We compare our results against a sample of optically bright, late-type galaxies (spirals) across the central 1.5 Mpc of the cluster taken from the *Arecibo Galaxy Environment Survey*. We find that these late-type spirals are predominantly found in the northern half of the cluster, especially those that are relatively gas rich. We calculate the H I deficiency and find that the expected global trend for the H I deficiency of these spirals to increase with projected proximity to the cluster core, seen in clusters like Coma and Virgo, is not observed. We classified the spirals into four evolutionary states, with the galaxies in each state sharing a similar degree of H I deficiency and optical colour. The common characteristics of the spirals in each evolutionary state suggest they have been subject to similar environmental processes. Many of the spirals in the most common evolutionary state (moderate H I deficiency and blue colour) have an H I intensity maximum which is displaced relative to its optical counterpart. The orientation of these offsets and magnitude of their H I deficiencies together with data from other wavelengths provide observational evidence in support of varying degrees of ram pressure stripping and tidal interaction. In general, our results indicate that the H I discs of bright late-type galaxies in the central part of the cluster are subject to both gas loss and morphological disturbance as a result of their interaction with the cluster environment. This provides further observational evidence of a more complex environment in Abell 1367 as compared to Virgo and Coma.

Key words: galaxies: clusters: individual: Abell 1367 – galaxies: evolution – galaxies: ISM.

1 INTRODUCTION

For several decades, it has been known that the fraction of spiral galaxies decreases when moving from a field population to a galaxy cluster core, with a corresponding increase in the fraction of early-type (E+S0) galaxies; this is known as the morphology–density relation (Dressler 1980; Oemler 1974). Whether this relation originates during galaxy formation or is mainly the result of environment remains one of the fundamental questions in observational cosmology. While previous work (Boselli & Gavazzi 2006; Dressler et al. 1999; Poggianti et al. 1999; Dressler 2004, and references therein) suggests that the environment associated with clusters only plays a

secondary role in producing lenticular galaxies from spirals, there is ample evidence for the effect of cluster environment on galaxy evolution, such as the observed increase in the fraction of H I-deficient spiral galaxies towards cluster cores (e.g. Boselli & Gavazzi 2006; van Gorkom 2004, and references therein), where the H I deficiency is defined as the log of the difference between the expected and observed H I mass (see Table 3, table footnote *h*). There is strong evidence that infalling cluster galaxies encountering a hot X-ray emitting intracluster medium (ICM) for the first time experience rapid evolution as a result (Gavazzi et al. 2001b; Sun & Murray 2002; Kenney, van Gorkom & Vollmer 2004; van Gorkom 2004). In these cases, the interaction removes the interstellar medium (ISM) from the galaxies (e.g. Gavazzi et al. 1995; Bravo-Alfaro et al. 2000; Solanes et al. 2001). For infalling spirals, the gas motions resulting

★E-mail: t.c.scott@herts.ac.uk

from the interaction are expected to lead to quenching of star formation, although modest and short time-scale (10^8 years) increases in star formation are predicted in specific circumstances (Fujita & Nagashima 1999; Kronberger et al. 2008). However, the predicted ram pressure induced star formation was not observed in a study by Iglesias-Páramo et al. (2004).

Different types of mechanisms are proposed to explain how the cluster environment impacts evolution of its constituent galaxies. The first type, which is most evident in spirals, consists of hydrodynamic mechanisms arising from gas-phase interactions between the cluster's hot ICM and a galaxy's ISM; these include ram pressure stripping (Gunn & Gott 1972), viscous stripping (Nulsen 1982), thermal evaporation (Cowie & Songaila 1977) and starvation (Bekki, Couch & Shioya 2002; Fujita & Goto 2004). The second type is caused by gravitational effects produced either by close encounters with neighbouring galaxies (merging or tidal stripping) or by repeated high-speed galaxy–galaxy encounters (*harassment*; Moore et al. 1996, 1999). Also in this category belongs a gravitational interaction between a galaxy and the cluster potential as a whole (Bekki 1999; Natarajan, Kneib & Smail 2002).

H I in spirals provides an excellent tool to investigate these mechanisms as it is sensitive to both gravitational and hydrodynamic interactions (Dickey & Gavazzi 1991). There is conflicting evidence for and against a correlation between the fraction of H I deficient galaxies and the cluster X-ray luminosity, L_X (Boselli & Gavazzi 2006; Giovanelli & Haynes 1985; Solanes et al. 2001). However, modelling by Tonnesen (2007) favours ICM stripping over gravitational effects as the primary cause of H I deficiency in nearby cluster spirals. Modelling of a generic spiral infalling to a cluster predicts the removal of almost all of its H I during the first transit of the cluster core as a result of hydrodynamic stripping. During the transit a combination of high ICM density and maximum orbital velocity hugely increases ram pressure stripping efficiency (Vollmer et al. 2001a; Roediger & Brügggen 2007). The few individually modelled spirals in Virgo, e.g. NGC 4522 (Kenney et al. 2004; Vollmer et al. 2008), NGC 4569 (Boselli et al. 2006; Vollmer et al. 2004) and in Coma NGC 4848 (Vollmer et al. 2001b), confirm that the ram pressure mechanism is operating. There are cases in Virgo, e.g. NGC 4654 (Vollmer 2003), NGC 4438 (Boselli et al. 2005), NGC 4254 (Chung et al. 2007; Chyży 2008) as well as examples in other clusters (Sun & Vikhlinin 2005; Moran et al. 2007), indicating that tidal mechanisms are operating in addition to hydrodynamic mechanisms.

The issue of galaxy evolution near clusters has become richer and more complex in recent years, since modelling suggests that under the hierarchical large-scale structure formation scenario clusters are expected to grow predominantly by accretion of groups of galaxies rather than individual galaxies (Blumenthal et al. 1984; Springel et al. 2001, although for an alternative model see Berrier et al. 2009). Infalling groups, having lower velocity dispersions than the clusters, provide opportunities for tidal interactions which may represent an important *pre-processing* stage in cluster galaxy evolution (Dressler 2004; Fujita & Goto 2004; Mihos 2004). Wilman et al. (2009) report strong evidence that transformation of spirals to S0s in clusters occurs preferentially in such groups as a result of tidal interactions at $z \sim 0.4$. Their results are based on analysis of *Hubble Space Telescope*–Advanced Camera for Surveys images of 179 spectroscopically confirmed group and 111 field galaxies from the Canadian Network for Cosmology (CNOC2) sample. This raises the question of what processes have perpetuated the transformation of late-type galaxies to S0s since then (Fasano et al. 2000), given in the current epoch hydrodynamic mechanisms appear to be the

predominant interaction type, but the most likely mechanisms for conversion of spirals to S0s are widely thought to be tidal (Dressler 1980; Bicker, Fritze-v. Alvensleben & Fricke 2002; Wilman et al. 2009).

In this paper, we consider A 1367 which together with A 1656 (the Coma cluster) comprises the Coma supercluster. A 1367 ($z = 0.022$) lies at the intersection of two filaments; the first extending 100 Mpc eastwards in the direction of the Virgo cluster and the second running NE towards Coma (West & Blakeslee 2000). A 1367, with a mean velocity ≈ 6240 km s $^{-1}$ and $\sigma \approx 822$ km s $^{-1}$, is an unrelaxed Bautz–Morgan type II–III, spiral rich, $6.9 \times 10^{14} M_{\odot}$ cluster (Boselli & Gavazzi 2006). Based on a redshift to the cluster of 0.022 and $\Omega_M = 0.3$, $\Omega_{\Lambda} = 0.7$ and $H_0 = 72$ km s $^{-1}$ Mpc $^{-1}$, the angular scale is 1 arcmin = 24.8 kpc.

A 1367 is, for several reasons, the perfect target to study environmental effects on spirals. It has a much higher fraction of spirals than its more massive neighbour Coma. X-ray observations of A 1367 carried out with *ASCA*, *XMM–Newton* (*XMM*) and *Chandra* indicate a dynamically young system with two principal subclusters (e.g. Donnelly et al. 1998). These two subclusters are themselves in the process of assembling from several smaller groups (Cortese et al. 2004). This suggests that A 1367 may be more like the unrelaxed clusters at earlier epochs than the more relaxed systems typical of low redshift (Oemler, Dressler & Butcher 1997). Being a lower mass cluster of the kind in which Poggianti et al. (2009) report enhanced rates of morphological transformation from spirals to S0s, it is potentially a location in which to test the mechanism leading to galaxy transformation suggested by Wilman et al. (2009). Furthermore, extensive optical and radio continuum studies have been carried out for A 1367. Gavazzi, in a series of papers (Gavazzi & Jaffe 1987; Gavazzi et al. 1995; Gavazzi & Boselli 1999; Gavazzi et al. 2001a), reported several galaxies with radio continuum and H α tails and exceptionally high star formation rates NW of the cluster centre, interpreted as arising from the interaction of galaxies with the cluster ICM. Also, the recently discovered blue infalling group (BIG), projected near the centre of A 1367 with a high relative velocity (Sakai et al. 2002; Gavazzi et al. 2003a; Cortese et al. 2006), may constitute a unique laboratory for testing *pre-processing* theories in cluster assembly.

This paper is the first stage of an investigation into the mechanisms transforming late-type galaxies in Abell 1367 which is focused on their H I content and position within the cluster. It is based on both Arecibo¹ single dish and National Radio Astronomy Observatory (NRAO)²–Very Large Array (VLA) synthesis H I imaging. Despite Arecibo's modest spatial resolution of ~ 3.5 arcmin, its homogeneous (in H I sensitivity) sky coverage, good sensitivity and high velocity resolution are well suited to study the global H I distribution throughout nearby clusters. But, interferometers, like the VLA, provide an order of magnitude better spatial resolution, and for nearby clusters the VLA's spatial resolution is sufficient to allow the effects of environment on the H I distribution in individual galaxies to be studied.

In this paper, we present the results of a VLA low/medium resolution H I spectral line study of two adjacent fields in the central and NW parts of A 1367. The H I imaging from these two fields covers a small fraction of the virial volume of the cluster.

¹ The Arecibo Observatory is part of the National Astronomy and Ionosphere Centre, which is operated by Cornell University under a cooperative agreement with the National Science Foundation.

² The NRAO is a facility of the National Science Foundation operated under cooperative agreement by Associated Universities, Inc.

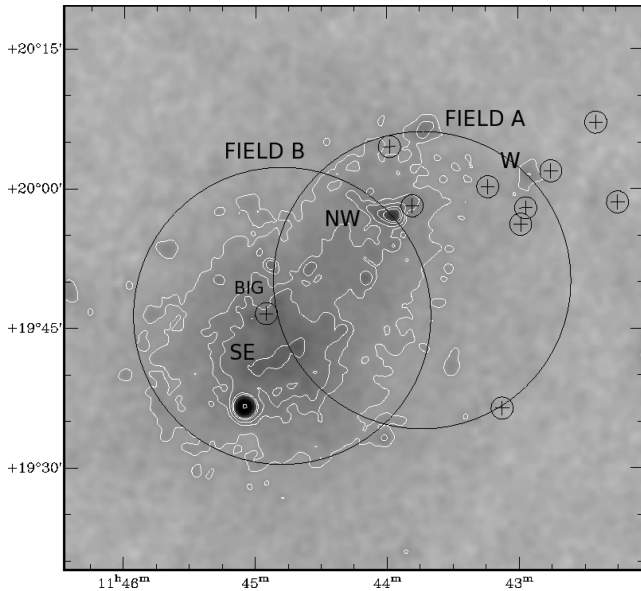


Figure 1. The positions of the two fields observed with the VLA are indicated by large circles showing the FWHM (32 arcmin) primary beams. VLA H I detections are shown with small black circles with crosses. The grey-scale is a *ROSAT* X-ray image with white contours overlaid. The positions of the SE, NW and W subclusters and the BIG compact group are labelled.

In Section 2, we give details of the VLA H I observations including data reduction. Special attention is given to the method we developed to optimize the continuum subtraction, leading to improved signal-to-noise ratio (S/N) for low-brightness H I features. We report our main observational results from the VLA H I imaging of individual galaxies in Section 3 and, in Section 4 the distribution of H I throughout the cluster volume from the Arecibo Galaxy Environment Survey (AGES) data. In Section 5, we discuss the implications of our data for evolutionary mechanisms in the cluster, based on the H I content and colour distributions at both large and small scales as well as on the peculiar H I morphologies shown by several galaxies. Our concluding remarks are given in Section 6.

2 OBSERVATIONS

We used two sets of VLA H I observations both of which are well within the 104 arcmin (2.58 Mpc) virial radius of the cluster (Moss 2006) and completely within the A 1367 AGES surveyed volume (Cortese et al. 2008). Fig. 1 indicates the FWHM primary beams for both VLA pointings (large circles). The figure also shows the intensity of the X-ray emission (*ROSAT*) from the cluster’s ICM (white contours) and the positions of the VLA H I detections (small black circles enclosing crosses). Observational parameters for both fields are listed in Table 1, including the velocity resolution, central velocities and the rms noise per field.

Table 1. VLA Observational parameters.

Field ^a	α_{2000} (^h ^m ^s)	δ_{2000} ([°] ['] ^{''})	Array configuration	Integration time (h)	Beam size (arcsec)	Velocity resolution (km s ⁻¹)	Central velocity (km s ⁻¹)	rms noise (mJy beam ⁻¹)	mJy conversion (K)
A	11 43 45.6	19 50 21	D	15.0	44 × 45	21	6800	0.27	0.3
B	11 44 50.0	19 47 00	C	3.6	15 × 15	11	8200	0.65	2.7

^aField A = VLA project ID: AB900; Field B = VLA project ID: AH801.

The sensitivity is non-uniform between the two VLA fields because of their differing array configurations and integration times. Additionally, for both fields, there is a sharp drop in sensitivity beyond the primary beam FWHM radius, significantly impacting the three detections in Field A furthest from the pointing centre.

2.1 VLA Field A – NW subcluster

Field A is centred near the NW subcluster (Cortese et al. 2004), ~10 arcmin NW of the cluster centre [position from NASA/IPAC Extragalactic Database (NED) between the NE and SE subclusters]. Field A’s position was chosen based on two considerations. First, the peculiar Zwicky infalling starburst galaxies CGCG 097-073, CGCG 097-079 and CGCG 097-087 were imaged within the 32 arcmin FWHM of Field A’s primary beam. Secondly, the first null of the beam was placed near 3C264 (a strong continuum source, with a flux density of 5 Jy at 1.4 GHz) to minimize the effects of its sidelobes.

This field was observed using the VLA in D configuration on 1999 March 26 and 30. Total observing time for the field was 15 h. We used correlator mode 4 which gives two independent intermediate frequencies (IFs), each with dual polarization (right- and left-hand circular). The IFs for the first day were set so that each IF generated a position–position–velocity subcube (α , δ , velocity) with a velocity range of ~500 km s⁻¹, with a small overlap between the velocity ranges. Combining the subcubes from both IFs produced a cube for the field with a velocity range of ~1000 km s⁻¹. The field was re-observed on the second day using the same procedure but for a range of velocities adjacent to that observed on the first day. When combined, the subcubes from both days produced a single cube of 96 channels with a continuous velocity range from 5762 to 7810 km s⁻¹ and a velocity width, using online Hanning smoothing, of 21 km s⁻¹ per channel. The final cube’s velocity range is more than twice the velocity dispersion of A 1367 (~822 km s⁻¹).

The data were calibrated and imaged following standard procedures using the AIPS software package. For Field A, self-calibration with a single iteration was carried out to improve upon the standard complex gain calibration. This was necessary to mitigate the effects of sidelobes from 3C264. We applied different robust weighting functions in the Fourier transform (AIPS task IMAGR), looking for a compromise between sensitivity and resolution. Our final data cubes were produced with robust weighting (using ROBUST = 0) and have a resolution of about 45 arcsec. The ROBUST option corrects the weights of the visibilities in the Fourier transform for the fact that there is a much higher density of measured visibilities in the inner part of the uv -plane compared to the outer regions (Briggs 1995). This comes at a cost of a slightly increased noise compared to using what is known as ‘natural weights’. For this data set, the H I mass detection threshold is $\sim 7 \times 10^7 M_{\odot}$ (corresponding to 3σ over two consecutive 21 km s⁻¹ channels). The equivalent column density sensitivity for emission filling the beam is then $1.9 \times 10^{19} \text{ cm}^{-2}$.

It was found that continuum subtraction was a critical step in the data reduction. Ordinarily, one would search for line-free channels in each subcube and then use, for example, `UVLIN` to subtract the continuum. The problem with our observations was that there was some H I emission at some position in almost every channel. This required a more elaborate approach consisting of deriving a continuum map made up of those areas on each channel map with no line emission and averaging them. This map was subsequently subtracted from the line + continuum data to produce cubes containing only line emission. In practice, this required the following procedure. First, continuum sources with peak flux density ≥ 10 mJy were modelled and removed in the *uv*-plane. This resulted in subcubes containing line and residual continuum sources of ≤ 10 mJy. In the second stage, AIPS tasks `SQASH` and `COMB` were used to create an average of all channels from the line plus residual continuum cube in the image plane, which was subtracted from the line plus residual continuum cube. This enabled us to find line-free channels in the subcubes, although in most cases there were very few (just 1 or 2). Continuum subtraction was then improved by repeating the subtraction but only using the average of these few line-free channels to produce subcubes with H I line emission only. The rms noise in these cubes was quite high because the continuum subtracted was based on very few channels.

In the final stage, these H I cubes were smoothed and blanked using AIPS tasks `CONVL` and `BLANK`, blanking out all areas in each channel containing line emission. These masks were in turn applied to the *line + residual* continuum subcubes to create, after again applying `SQASH`, residual continuum-only maps for each of the subcubes. These residual continuum maps were then subtracted from the original *line + residual* continuum subcubes, resulting in subcubes with only H I emission, but with a much reduced rms noise. The continuum-subtracted subcubes were subsequently combined with `MCUBE`. The final cube produced in this way had a noise of ~ 0.27 mJy beam $^{-1}$ which increased the number of H I detections by 50 per cent compared to the equivalent cube produced using `UVLIN`.

2.2 VLA Field B – BIG

The second set of VLA H I observations was centred on the BIG (Fig. 1), overlapping slightly and located to the SE of Field A, with a central velocity of 8200 km s $^{-1}$, i.e. the mean velocity of the BIG galaxies. Archival C-array observations (correlator mode 2 with online Hanning smoothing) from 2002 December 8 were used to produce an image cube with 48 channels (after discarding the noisy edge channels) with a velocity width of 11 km s $^{-1}$ per channel. The velocity coverage was 7913–8587 km s $^{-1}$. Our final data cube has a resolution of ~ 15 arcsec. In the spatial overlap region between the two observed VLA fields, the velocity range extends from 5762 to 8587 km s $^{-1}$ (except for a narrow gap at ~ 7900 km s $^{-1}$). For Field B, the equivalent H I mass detection threshold is $\sim 8 \times 10^7 M_{\odot}$ (corresponding to 3σ in 2 consecutive 11 km s $^{-1}$ channels). This is equivalent to column density sensitivity for emission filling the beam of 2.1×10^{20} cm $^{-2}$.

3 OBSERVATIONAL RESULTS

3.1 The H I in individual galaxies: VLA observations

Nine objects were detected in Field A (NW and W subclusters; Cortese et al. 2004) and two more within Field B (BIG). Channel

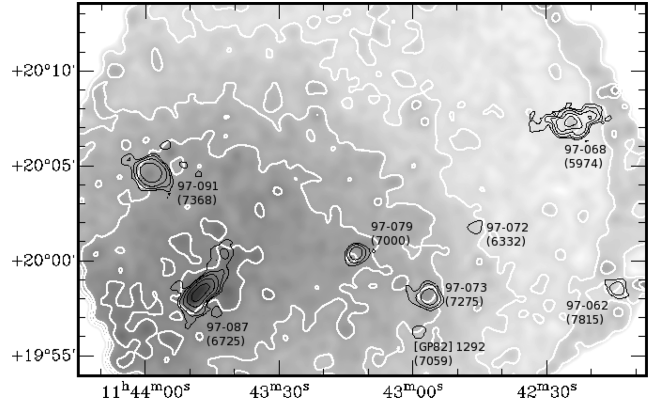


Figure 2. NW region of A 1367: X-ray emission (*XMM*) image with white contours. Black contours indicate H I emission from the VLA H I detections in Field A, with the outer contour indicating a column density of $N_{\text{H I}} = 3 \times 10^{19}$ cm $^{-2}$. Values in parentheses below the Zwicky identifier are optical velocities in km s $^{-1}$.

maps for each detected object are available in Appendix C (online material – see the Supporting Information). Fig. 2 shows the VLA H I detections in the NW area of the cluster and their locations relative to X-ray emission (from *XMM–Newton*). The *XMM–Newton* archive data were derived from an observation taken on 2001 November 22. After standard flare filtering, the exposure time was 20.6 ks for the pn and 29.9 ks for the two MOS cameras. Images in the 0.5–5.0 keV energy band were derived by combining the exposure-corrected images from all three cameras and convolving with a Gaussian.

The morphological type, equivalent width of the H α line EW (H α), VLA H I velocity including uncertainty, $\Delta V_{\text{H I}}$ including uncertainty, H I mass and offset (of the H I compared to the optical position) for the VLA detections are given in Table 2.

The uncertainty in position for sources in the VLA fields is ~ 4 arcsec (1.6 kpc) and 2 arcsec (0.8 kpc) for Field A and B, respectively, i.e. uncertainties are $\sim 1/10$ th of the synthesized beam. Within a velocity-integrated intensity map of an individual spiral, positional uncertainty varies depending on S/N. This means positional uncertainty within a map of a spiral is lowest in the region of velocity-integrated intensity maximum. But, we caution that the distribution beyond the H I intensity maximum region in spirals beyond the FWHM of the primary beam is more uncertain.

Four galaxies, CGCG 097-062, CGCG 097-068, CGCG 097-072 and CGCG 097-125, imaged with the VLA have their H I intensity maximum offset relative to their optical counterpart (final column of Table 2) in directions which are not radial with respect to the cluster centre, i.e. these cases are inconsistent with a simple ram pressure scenario. The direction of these offsets may arise from a tidal interaction or a more complex ram pressure scenario such as gas fallback (see Section 3.3 for CGCG 097-072).

Most of the galaxies have previously been detected in H I with Arecibo (Chincarini et al. 1983; Giovanelli & Haynes 1985; Gavazzi 1989; Springob, Haynes & Giovanelli 2005) and/or with the VLA (Dickey & Gavazzi 1991; Hota & Saikia 2007). None of the authors showed H I maps of their detected galaxies because of insufficient resolution or sensitivity, except Hota & Saikia (2007) who presented H I maps of the three most active starburst galaxies.

All objects in Table 2 were also detected in AGES (Table 3 and Cortese et al. 2008), with total fluxes and velocities generally in good agreement with ours. As an example we show, in Fig. 3, a comparison of the AGES and VLA Field A spectra for a detection

Table 2. Parameters for the VLA H_I detected galaxies.

ID ^a	α_{2000}^b (^h m ^s)	δ_{2000} ([°] / ^{''})	Type ^c	EW (H α) ^d (Å)	$V_{\text{H I}}^e$ (km s ⁻¹)	$\sigma(V_{\text{H I}})^f$ (km s ⁻¹)	W_{20} (km s ⁻¹)	$\Delta V_{2\sigma}^g$ (km s ⁻¹)	$\sigma(\Delta V_{2\sigma})^h$ (km s ⁻¹)	$M_{\text{H I}}^i$ (10 ⁹ M _⊙)	Offset ^j
97-068	11 42 24.5	20 07 10	Sbc	41	5958 ± 5		346	346 ± 10	6.9	15 arcsec	N
GP1227	11 43 13.0	19 36 47	Dw*	30	6239 ± 11		86	86 ± 22	0.9	none	
97-072	11 42 45.2	20 01 57	Sa	9	6207 ± 4		64	64 ± 9	0.4	12 arcsec	SE
97-087	11 43 49.1	19 58 06	Im	77	6738 ± 27		563	649 ± 54	8.0	30 arcsec	NW
97-079	11 43 13.4	20 00 17	Irr	129	7019 ± 21		216	216 ± 41	1.3	10 arcsec	NW
GP1292	11 42 58.9	19 56 12	Dw*	–	7203 ± 23		64	64 ± 46	0.3	none	
97-073	11 42 56.4	19 57 58	SA:pec	111	7301 ± 11		173	216 ± 22	2.0	8 arcsec	N
97-091	11 43 59.0	20 04 37	Sa	23	7377 ± 2		259	281 ± 4	5.3	none	
97-062	11 42 14.8	19 58 35	Sa:pec	37	7723 ± 13		64	64 ± 26	0.7	15 arcsec	SW
97-125	11 44 54.8	19 46 35	S0a	23	8158 ± 18		206	206 ± 35	1.3	12 arcsec	SW
K2	11 44 50.6	19 46 02	H II	–	8158 ± 12		162	162 ± 24	–	–	–

^aZwicky catalogue, except GP1277 = Abell 1367[GP82]1227 and GP1292 = Abell 1367[GP82]1292.

^bOptical galaxy position from NED.

^cHubble classification from NED; * = our classification.

^dEW(H α) is from GOLDMine, except GP1227 which is our measurement.

^eVelocity = the mean of the upper and lower velocity defined by the linewidth (see the note g).

^fUncertainty for $V_{\text{H I}} = 1.5 (W_{20} - W_{50})(S/N)^{-1}$ (Schneider et al. 1990), except where $W_{20} = W_{50}$ in which case $\sigma(V_{\text{H I}}) = 1.5 (2 \times \text{channel width})(S/N)^{-1}$.

^gThe velocity width based on the number of contiguous channels with $\geq 2\sigma$ detections.

^hUncertainty in the line width = $2\sigma(V_{\text{H I}})$.

ⁱ $M_{\text{H I}} = 2.36 \times 10^2 D^2 S_{\text{H I}}$ where $M_{\text{H I}}$ is in M_⊙, D in Mpc and $S_{\text{H I}}$ is the VLA flux in mJy km s⁻¹. Mass based on a distance of 91.6 Mpc ($V_{A1367} = 6595$ km s⁻¹ from NED and $H_0 = 72$ km s⁻¹ Mpc⁻¹).

^jThe offset direction is the projected position of the H_I intensity maximum relative to its optical counterpart, except for CGCG 097-087 where the direction and distance are taken from the NIR counterpart. The projected distance between the two intensity maxima is given in arcsec with a positional uncertainty of ~ 4 arcsec.

well within the VLA FWHM beam. Important exceptions to this agreement include CGCG 097-073 and A 1367 [GP82]1292, which are confused in the AGES beam but are resolved by the VLA.

While the determination of velocity for each channels is accurate to within a few km s⁻¹, the range of velocities detected for each galaxy depends on sensitivity. The VLA detections of CGCG 097-068, CGCG 097-072 and CGCG 097-062 are beyond the Field A primary beam, where not only is the sensitivity lower than in AGES but the fluxes are more uncertain due to the limited knowledge of the VLA primary beam beyond the half-power radius. For example, the noise at the position of CGCG 097-068 is approximately five times greater than at the centre of the primary beam.

In the following sections, we describe the most notable features of the VLA detections. The images displayed here were produced after applying a primary beam correction. The α and δ axes of all maps are in J2000 coordinates.

3.2 The star-forming galaxies (CGCG 097-087, CGCG 097-073 and CGCG 097-079)

These three starburst galaxies have been extensively studied in the past (Nulsen 1982; Gavazzi et al. 1984; Gavazzi & Jaffe 1987; Gavazzi 1989; Dickey & Gavazzi 1991; Boselli et al. 1994; Gavazzi et al. 1995, 2001a,b; Hota & Saikia 2007). They all have exceptionally high star formation rates, $\text{EW}(\text{H}\alpha + [\text{N II}]) > 75 \text{ \AA}$ (Table 2), and display spectacular radio continuum and H α tails pointing away from the cluster centre (Gavazzi & Jaffe 1987; Gavazzi et al. 2001b). Some observational features of these three objects have been interpreted as effects of ram pressure stripping produced by the ICM, in particular the enhanced star formation activity and the displacement of atomic hydrogen relative to their stellar discs, although in the case of CGCG 097-087 much of the enhanced star formation rate is probably attributable to a merger (Gavazzi et al. 2001a; Martig &

Bournaud 2008). The H_I in the central parts of these starbursts has been recently mapped by Hota & Saikia (2007). The maps presented here, though, show additional large-scale H_I features as a result of our improved continuum subtraction (see Section 2.1).

(i) CGCG 097-087: the integrated H_I map (Fig. 4) shows the H_I intensity maximum is offset by ~ 30 arcsec (12 kpc) to the NW of the nucleus, confirming the H_I is asymmetrically distributed, as earlier reported by Gavazzi (1989) and Dickey & Gavazzi (1991). Higher spatial resolution and lower sensitivity H_I maps have previously been presented for the inner parts of this galaxy by Hota & Saikia (2007). The main body of the galaxy displays rotation in the velocity range ~ 6500 – 6900 km s⁻¹ (Fig. 5). We do not see the jump in velocities observed in H α and CO (Boselli et al. 1994; Gavazzi et al. 2001a), but this may be due to our low spatial resolution. We are not able to confirm the merger hypothesis suggested by the H α kinematics (Gavazzi et al. 2001a; Amram et al. 2002), but the H_I velocity field has a much steeper velocity gradient SE of the nucleus, coinciding with the disturbed optical disc. We also see that the H_I disc is sharply truncated, with its SE edge approximately coinciding with the edge of the optical disc. An impressive H_I tail, coinciding with the radio continuum tail (Gavazzi et al. 1995), extends at least 70 kpc to the NW of the nucleus, with an increasing offset from the plane of the optical galaxy. At the end of this tail, the H_I map shows a clump without an optical counterpart. The clump has a velocity width of ~ 100 km s⁻¹.

(ii) CGCG 097-073 and A 1367 [GP82]1292: Fig. 6 shows the H_I in CGCG 097-073 having a slightly asymmetric distribution, the intensity maximum being displaced ~ 8 arcsec (3 kpc) to the north of the optical disc, confirming the earlier report of H_I asymmetry (Dickey & Gavazzi 1991). The H_I displacement is in the same direction as the H α and radio continuum tails (Gavazzi et al. 1995, 2001b). H_I does not appear truncated, which is consistent with

Table 3. Parameters for the brightest late-type galaxies in A 1367.

ID ^a	α_{2000}^b (hms)	δ_{2000} (° ' ")	Optical ^c velocity (km s ⁻¹)	<i>i</i> -band ^d (mag)	$g - i^e$ (mag)	Major ^f axis (arcmin)	Type ^g	H I def ^h	Companion ⁱ separation (km s ⁻¹) (arcsec)	State ^j
97-064	11 42 14.61	20 05 52.18	5976	14.18	1.06	0.65	S (dS)	≥0.48	– –	B
97-062	11 42 14.78	19 58 35.5	7815	14.78	0.62	1.01	Pec	0.35	– –	A
97-063	11 42 15.62	20 02 55.24	6102	15.27	0.63	0.58	Pec	0.01	– –	A
97-068	11 42 24.49	20 07 09.55	5974	13.24	0.99	1.23	Sbc	−0.28	– –	B
97-072	11 42 45.16	20 01 56.35	6332	13.61	1.07	1.21	Sa	0.55	– –	B
97-073	11 42 56.45	19 57 58.39	7275	15.08	0.55	0.76	Pec	0.02	– –	A
97-076	11 43 02.14	19 38 59.02	6987	13.56	1.17	1.20	Sb	≥0.88	– –	D
97-079	11 43 13.08	20 00 17.46	7000	14.37	0.47	0.75	Pec	0.25	– –	A
97-078	11 43 16.22	19 44 55.46	7542	13.55	1.21	1.88	Sa	≥0.96	– –	D
97-082	11 43 24.55	19 44 59.35	6100	13.00	1.20	1.30	Sa	≥0.77	– –	D
97-087	11 43 49.07	19 58 06.49	6725	13.19	0.64	2.00	Pec	0.39	– –	A
97-092-NED1	11 43 58.2	20 11 08	6487	14.95	0.99	0.76	Sbc	≥0.62	– –	B
97-091	11 43 58.96	20 04 37.34	7368	13.26	0.99	1.12	Sa	−0.23	– –	B
97-093	11 44 01.95	19 47 03.94	4909	15.05	0.42	0.96	Pec	≥0.78	– –	D
97-102-NED2	11 44 16.49	20 13 00.73	6364	13.67	1.24	1.08	Sa	0.41	4 24	C
97-111 NED1	11 44 25.93	20 06 09.64	7436	14.92	1.14	0.45	Irr	≥0.21	194 24	C
97-121	11 44 47.04	20 07 30.32	6571	12.86	1.18	1.20	Sab	0.38	– –	C
97-114	11 44 47.8	19 46 24.31	8293	15.12	0.57	0.54	Pec	≥0.34	22 102	–
97-119	11 44 47.95	19 41 18.56	4895	14.18	0.98	0.60	Sa	≥0.37	– –	–
97-120	11 44 49.16	19 47 42.14	5595	12.53	1.12	1.32	Sa	≥0.78	– –	D
97-122	11 44 52.23	19 27 15.12	5468	13.65	0.93	1.45	Pec	0.47	– –	B
97-125	11 44 54.85	19 46 35.18	8271	13.81	1.20	0.84	S0a	≥−0.14	22 102	–
97-129-NED1	11 45 03.88	19 58 25.24	5085	12.29	1.21	2.36	Sb	−0.07	– –	C
97-138	11 45 44.6	20 01 50.8	5313	13.99	0.42	0.75	Pec	−0.12	– –	A
BO85 074	11 45 06.57	20 09 23.21	6151	14.69	1.03	0.38	S	0.08	– –	B
97-129 NED2	11 45 06.95	19 58 0.66	7546	14.66	1.12	1.07	Sbc	≥0.8	– –	D

^aZwicky catalogue, except [BO85]074 from Butcher & Oemler (1985), with the suffixes indicating the NED pair identifier.

^bOptical galaxy positions ex SDSS Data Release 6 (DR6).

^cFrom NED.

^dex SDSS DR6.

^eex SDSS DR6.

^fex GOLDMine except CGCG 097-111 and [BO85]074 which are taken from NED.

^gex GOLDMine except [BO85]074 which is taken from NED.

^hH I deficiency is calculated using the method of Haynes & Giovanelli (1984) and the parameters from Solanes et al. (1996), using total H I flux measurements from AGES and galaxy diameters equal to the major axis diameter from GOLDMine (except [BO85]074 which is taken from NED). For 97-079, the mass was calculated from our VLA total flux because the AGES flux was affected by RFI. For AGES non-detections, the H I deficiency lower limit was calculated using the AGES detection limit of $6 \times 10^8 M_{\odot}$. No H I deficiency could be calculated for CGCG 097-119 because flux from this galaxy was confused in the AGES beam with 3C264. The calculated H I deficiencies are highly uncertain because of the intrinsic spread in H I properties of individual spirals and we adopt an uncertainty of ± 0.3 dex throughout this paper.

ⁱA galaxy is considered to be a likely companion if its separation is ≤ 2 arcmin, the velocity difference is ≤ 500 km s⁻¹ and the companion has a diameter ≥ 0.5 arcmin.

^jEvolutionary state described in Section 5.3.

the normal H I content (H I deficiency = 0.02). Also shown in the same figure is an H I detection at the position of the blue dwarf galaxy Abell [GP82]1292 which appears undisturbed. Given the projected distance of ~ 1.9 arcmin (47 kpc) and the 11 km s⁻¹ velocity separation between the two (perturbation parameter $p_{gg}^3 \sim 0.004$), a gravitational interaction cannot be ruled out.

(iii) CGCG 097-079: H I has been previously detected in this galaxy (Gavazzi 1989; Dickey & Gavazzi 1991). Fig. 7 shows the H I to be symmetrically distributed but with the intensity maximum displaced by ~ 10 arcsec (4 kpc) to the NW of the optical disc, as previously reported by Gavazzi (1989) and Hota & Saikia (2007).

³ $p_{gg} = \frac{(M_{\text{comp}}/M_{\text{gal}})}{(d/r_{\text{gal}})^3}$, where M_{gal} and M_{comp} are the masses of the galaxy and companion, respectively, d is the separation and r is the galaxy disc radius (Byrd & Valtonen 1990).

The H I offset is in the same direction as the H α and radio continuum tails (Gavazzi et al. 1995, 2001b).

3.3 Giant late-type galaxies (CGCG 097-062, CGCG 097-068, CGCG 097-072 and CGCG 097-091)

In addition to the three starbursts, we were able to map four more spirals in the NW and W subclusters (Fig. 2).

(i) CGCG 097-062: this optically asymmetric, Sbc (NED) or Pec (GOLDMine⁴), galaxy is well beyond Field A's FWHP beam, but our weak H I detection is consistent with the H I deficiency (AGES) of 0.35. Fig. 8 shows the H I intensity maximum displaced ~ 15 arcsec (6 kpc) to the SW of its optical counterpart, in the

⁴ Galaxy On Line Database Milano Network; <http://goldmine.mib.infn.it/>

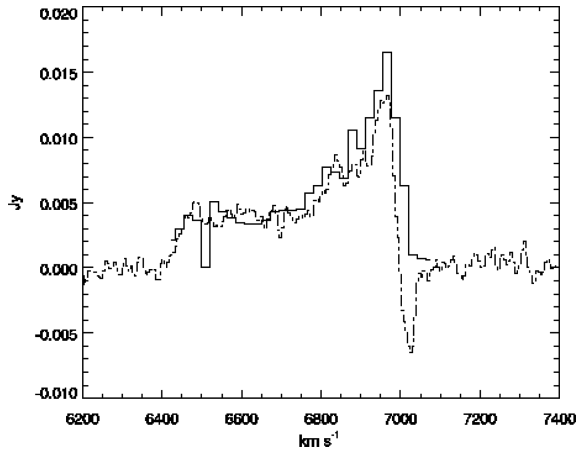


Figure 3. CGCG 097-087 VLA (solid line) and AGES (dashed line), integrated H I spectra. The feature at 7000 km s^{-1} in the AGES spectrum is an RFI artefact.

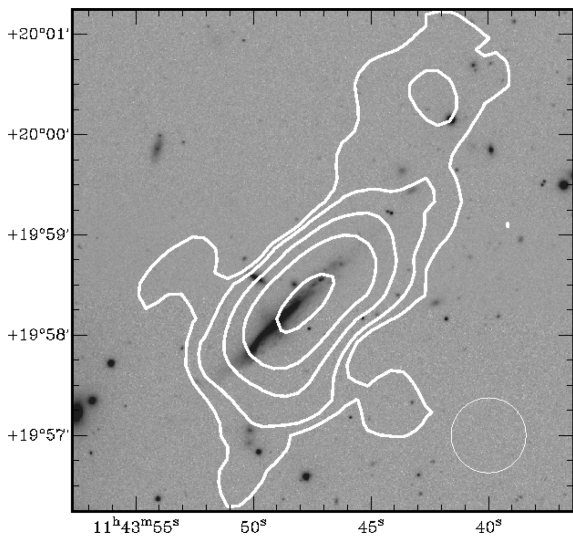


Figure 4. CGCG 097-087: white contours are from a robust 0 H I surface density map, with the outer contour indicating a column density of $N_{\text{H I}} = 3 \times 10^{19} \text{ cm}^{-2}$, with higher levels at $8, 20, 40$ and $80 \times 10^{19} \text{ cm}^{-2}$, overlaid on an SDSS *i*-band image. The first contour also corresponds to a 8σ detection in three channels. The size of the D-array beam is indicated with the white circle.

direction of the optical tail. CGCG 097-062, like CGCG 097-087, has a pronounced asymmetric H I spectrum (Gavazzi 1989).

(ii) CGCG 097-068: despite its position well beyond the FWHP region of the VLA's primary beam, CGCG 097-068's H I signal was sufficient to show a double-peaked VLA spectrum which approximately matches its AGES counterpart, strongly suggesting that this massive Sbc galaxy is inclined and H I rich (H I deficiency of -0.28 ; Table 3). This galaxy was tentatively reported as having its H I intensity maximum displaced north of the optical disc (Dickey & Gavazzi 1991). The position of the VLA H I intensity maximum ~ 15 arcsec (6 kpc) in projection north of the optical nucleus confirms this (Fig. 9).

(iii) CGCG 097-072: this Sa galaxy lies, in projection, close to the W subcluster galaxy density maximum (Cortese et al. 2004). Our H I detection is weak, consistent with its high H I deficiency of 0.55 (AGES). Fig. 10 shows an H I intensity maximum offset ~ 12 arcsec (5 kpc) to the SE of the optical nucleus, and suggests

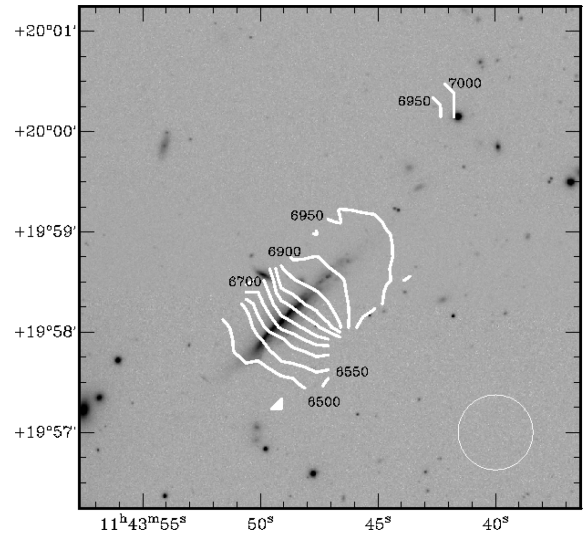


Figure 5. CGCG 097-087 velocity field: white contours show velocities from 6500 to 7000 km s^{-1} , in 50 km s^{-1} steps based on the robust 0 cube overlaid on an SDSS *i*-band image. The size of the D-array beam is indicated with the white circle.

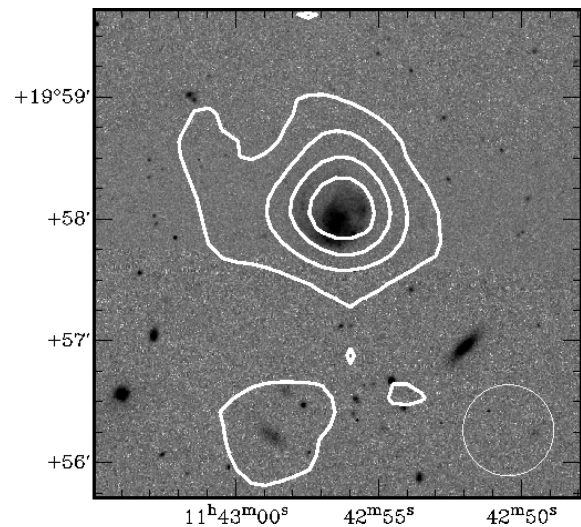


Figure 6. CGCG 097-073 (upper contour) and A 1367 [GP82]1292 (lower contour): contours trace the robust 0 H I surface density, with the outer contour indicating a column density of $N_{\text{H I}} = 3 \times 10^{19} \text{ cm}^{-2}$, with higher levels at $10, 17$ and $24 \times 10^{19} \text{ cm}^{-2}$ overlaid on an SDSS *i*-band image. The first contour also corresponds to a 7σ detection in three channels. The size of the D-array beam is indicated with the white circle.

a truncated H I disc. However, this requires further confirmation as the galaxy is beyond the FWHP beam of Field A. The high H I deficiency and anomalous direction of its H I displacement relative to that seen in nearby spirals is similar to NGC 4848 in Coma where a truncated H I disc was reported by Bravo-Alfaro et al. (2001) and further CO imaging and numerical simulations by Vollmer et al. (2001b) revealed a case of gas fallback.

(iv) CGCG 097-091: H I has been previously detected in this galaxy with Arecibo and the VLA (Dickey & Gavazzi 1991), but was not spatially resolved. The AGES H I deficiency of -0.23 shows the galaxy to be H I rich. CGCG 097-091 has the most symmetric H I morphology of our VLA detections, with a near perfect coincidence of position and velocity between the optical nucleus and

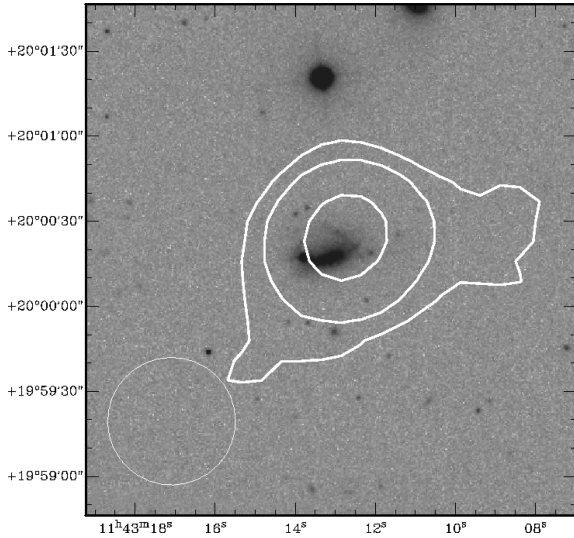


Figure 7. CGCG 097-079: white contours are from a robust 0 H I surface density map, with the outer contour indicating a column density of $N_{\text{H I}} = 3 \times 10^{19}$ atoms cm^{-2} , followed by contours at 10 and 17×10^{19} atoms cm^{-2} on an SDSS *i*-band image. The first contour also corresponds to a 7σ detection in three channels. The size of the D-array beam is indicated with the white circle.

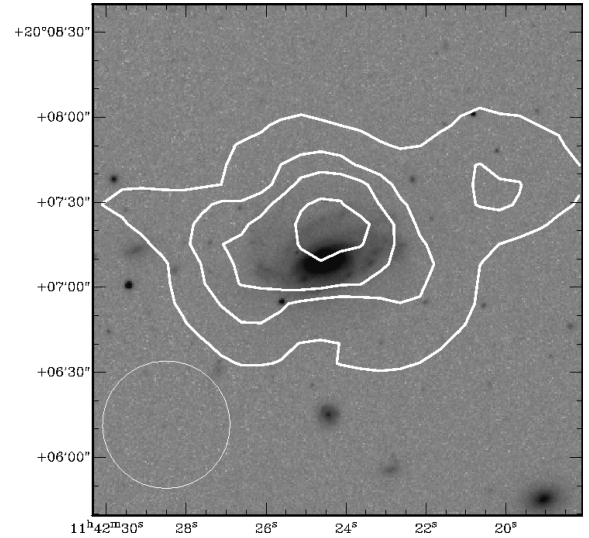


Figure 9. CGCG 097-068: white contours are from a robust 0 H I surface density map, with the outer contour indicating a column density of $N_{\text{H I}} = 10 \times 10^{19}$ atoms cm^{-2} , higher levels at 30 , 50 and 70×10^{19} atoms cm^{-2} on an SDSS *i*-band image. The first contour also corresponds to a 5σ detection in three channels. The size of the D-array beam is indicated with the white circle.

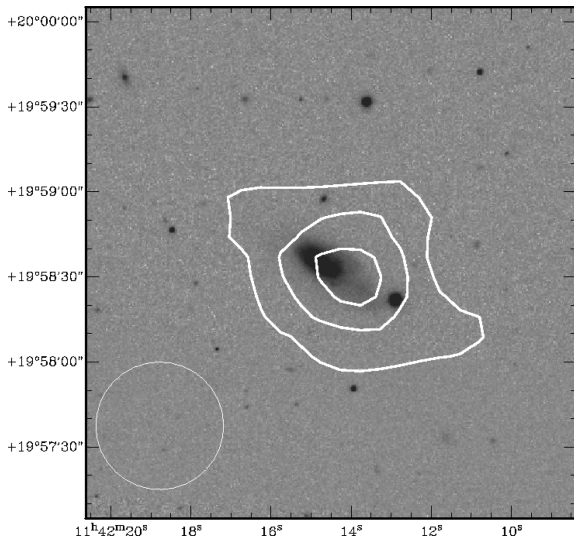


Figure 8. CGCG 097-062: white contours are robust 0 H I surface density levels with the outer contour corresponding to a column density of $N_{\text{H I}} = 3 \times 10^{19}$ atoms cm^{-2} , with higher levels at 8 and 13×10^{19} atoms cm^{-2} , on an SDSS *i*-band image. The first contour also corresponds to a 2σ detection in three channels. The size of the D-array beam is indicated with the white circle.

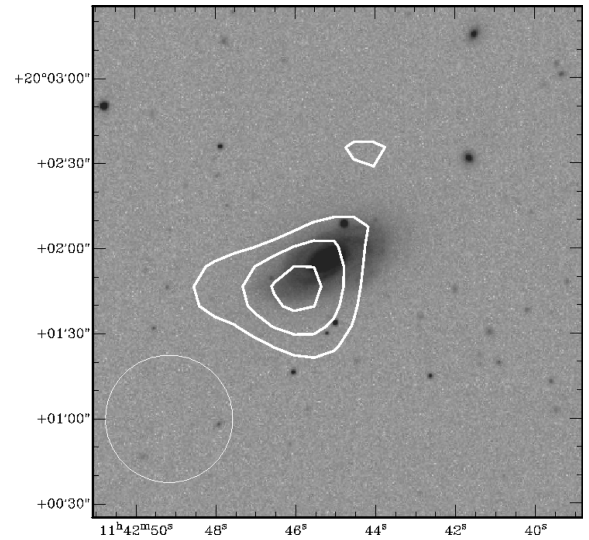


Figure 10. CGCG 097-072: white contours are from a robust 0 H I surface density map, with the outer contour indicating a column density of $N_{\text{H I}} = 3 \times 10^{19}$ atoms cm^{-2} and the higher contours are 5 and 7×10^{19} atoms cm^{-2} , on an SDSS *i*-band image. The first contour also corresponds to a 4σ detection in three channels. The size of the D-array beam is indicated with the white circle.

the H I intensity maximum (Tables 2 and 3). These characteristics together with the velocity field (Fig. 11), which shows normal rotation, combine to suggest CGCG 097-91 is a normal spiral which is not interacting with its environment in any significant way.

3.4 The H I around the blue infalling group

Our VLA H I observation of the BIG (Field B) has a higher spatial resolution (~ 15 arcsec), compared to Field A (~ 45 arcsec), but at significantly lower sensitivity because of the shorter integration time. The strongest detection in Field B is near the disturbed

S0a galaxy CGCG 097-125, and we confirm that the H I intensity maximum is offset ~ 12 arcsec (5 kpc) westwards from the optical centre (Fig. 12). The high column density H I to which Field B is sensitive is asymmetrically distributed with its major axis running approximately SE–NW. Comparing our H I images to the earlier more sensitive observations by Sakai et al. (2002) with the Westerbork Synthesis Radio Telescope (WSRT) indicates that the BIG contains extensive diffuse H I, which our observation was not sensitive enough to detect. Comparison between our H I spectrum and AGES confirms the presence of this diffuse H I in the velocity range

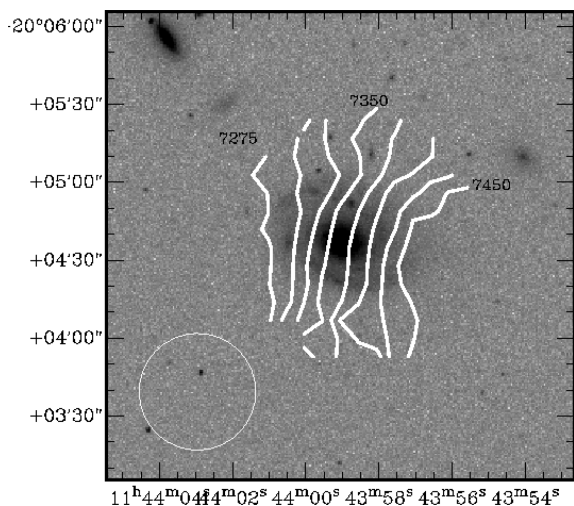


Figure 11. CGCG 097-091 H I velocity field: based on a robust 0 cube, contours are 7275, 7300, 7325, 7350, 7375, 7400, 7425 and 7450 km s⁻¹ on an SDSS *r*-band image. The size of the D-array beam is indicated with the white circle.

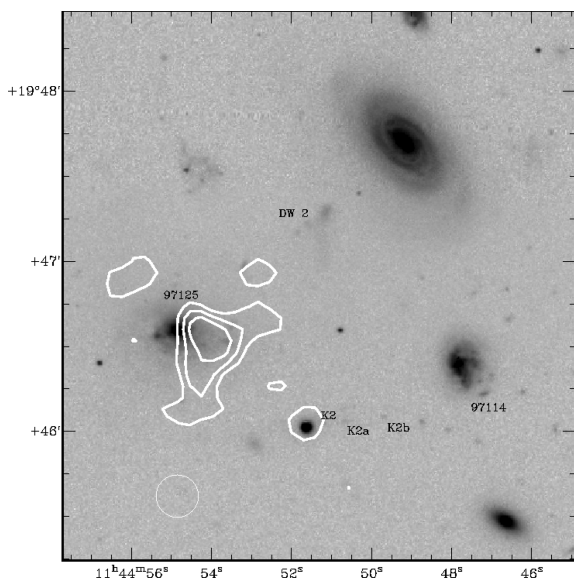


Figure 12. CGCG 097-125 and knot near K2: white contours are from a robust 0 H I surface density map, with the outer contour indicating a column density of $N_{\text{H I}} = 4 \times 10^{20} \text{ cm}^{-2}$, higher levels are at 8 and $12 \times 10^{20} \text{ cm}^{-2}$ on an SDSS *g*-band image. The first contour also corresponds to a 4σ detection in three channels. The size of the C-array beam is indicated with the white circle.

from 8000 to 8500 km s⁻¹. Further details of our observation of the BIG can be found in Appendix A.

3.5 Dwarf galaxy A 1367 [GP82]1227

This isolated irregular dwarf galaxy is detected in H I, both by the VLA and in AGES, to the SW of the cluster centre in a region otherwise devoid of H I detections (Fig. 13). The VLA and AGES H I spectra are in good agreement and display a single narrow peak ($W_{50} = 56 \pm 8 \text{ km s}^{-1}$; Cortese et al. 2008), typical of a dwarf irregular galaxy. The VLA observations show the H I intensity maximum is offset 3 arcsec (1 kpc) to the south of its optical counterpart.

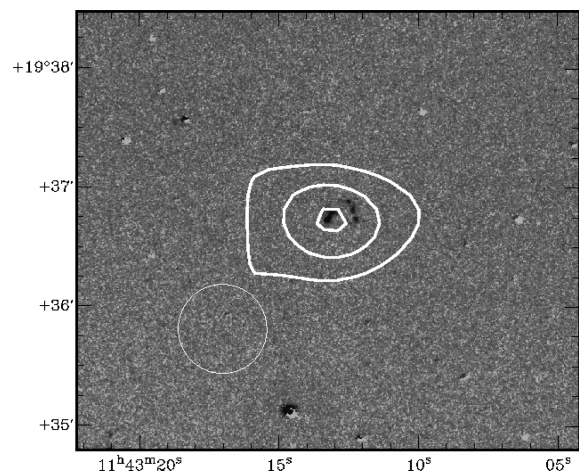


Figure 13. [GP82]1227: white contours are from a robust 0 H I surface density map. The outer contour is $N_{\text{H I}} = 3 \times 10^{19} \text{ cm}^{-2}$, higher levels are at 10 and $17 \times 10^{19} \text{ cm}^{-2}$, overlaid on an H α image. The first contour also corresponds to a 4σ detection in three channels. The size of the D-array beam is indicated with the white circle.

Details of a low-resolution optical spectrum obtained for this galaxy can be found in Appendix B.

4 H I (AGES) AND COLOUR DISTRIBUTION IN A 1367

To place our VLA observations in context, we used the AGES H I survey together with Sloan Digital Sky Survey (SDSS) data to analyse the H I content and colour of bright late-type galaxies throughout the central volume of the cluster (including the VLA fields).

As part of the AGES project, the 305-m Arecibo Telescope was used to survey H I in a volume centred on A 1367 covering about 5 deg², between $11^{\text{h}}34^{\text{m}}00^{\text{s}} < \alpha_{2000} < 11^{\text{h}}54^{\text{m}}15^{\text{s}}$, $19^{\circ}15' < \delta_{2000} < 20^{\circ}20'$, in a velocity range $\sim 1100\text{--}19000 \text{ km s}^{-1}$ (Cortese et al. 2008). The survey has an angular resolution of $3.3 \times 3.8 \text{ arcmin}$ and a velocity resolution of $\sim 10 \text{ km s}^{-1}$ with a mass sensitivity limit of $6 \times 10^8 M_{\odot}$ of H I over a velocity $W_{50} = 200 \text{ km s}^{-1}$. Positional uncertainties for the detections are estimated to be $\sim 18 \text{ arcsec}$ ($\sim 7 \text{ kpc}$). The observations were made in drift scan mode providing a consistent flux-limited H I detection threshold throughout the AGES volume. The observations and data reduction process is described in Auld et al. (2006). More details on this survey are given in Cortese et al. (2008).

In the field, significant amounts of H I are expected to be present in the discs of both spiral and dwarf galaxies. In the case of spirals, the amount of H I can be approximately related to the optical disc diameter and the galaxy's morphological type (Haynes & Giovanelli 1984; Solanes, Giovanelli & Haynes 1996), but for dwarfs the H I mass fraction is both larger and more uncertain. The AGES detection limit implies that spiral galaxies in A 1367 with an optical disc diameter $< 0.37 \text{ arcmin}$ ($\sim 9 \text{ kpc}$) would not be detected in AGES (Solanes et al. 1996; Cortese et al. 2008). Galaxies with disc diameters below this limit are almost certainly dwarfs, so that AGES is essentially only sensitive to H I in late-type spiral galaxies of A 1367. However, two dwarf galaxies were detected within our sampled volume, showing that AGES includes galaxies from the high end of the dwarf H I mass function.

AGES allows us to investigate the H I deficiency of A 1367's spirals, down to its sensitivity limit, by comparing their expected

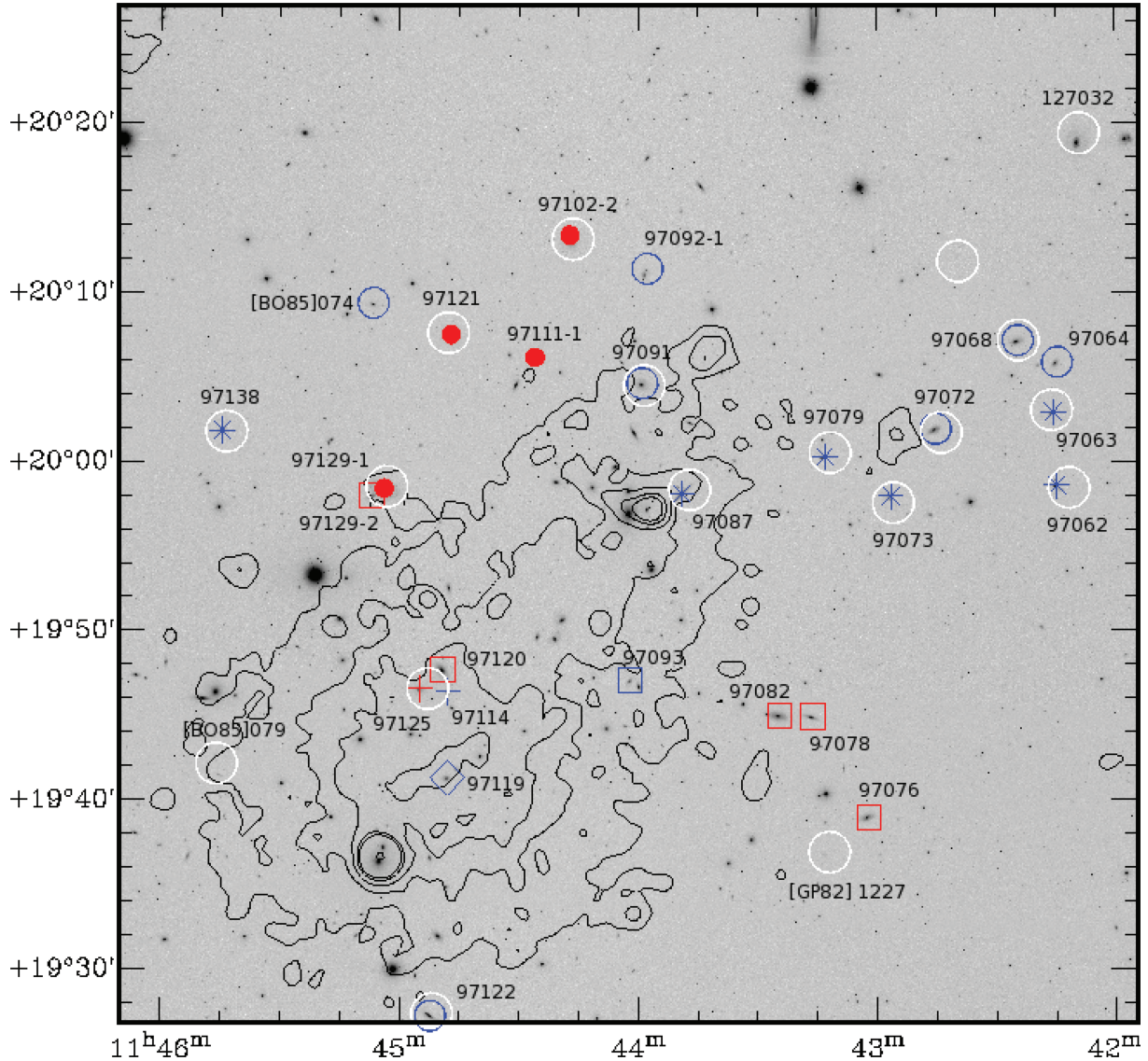


Figure 14. Positions of selected late-type galaxies in the volume sampled. The *colour* of the symbol (red or blue) used for each spiral indicates its SDSS $g - i$ colour: blue (≤ 1.1), red (> 1.1). AGES H I detections are marked (white circles). The *symbol* used for each spiral indicates its evolutionary state (discussed in Section 5.3) as follows: A (asterisk), B (open circle), C (filled circle) and D (open square), BIG spirals (cross) and unclassified (diamond). ROSAT X-ray intensities (black contours) are overlaid on an SDSS i -band image. Details for the galaxy identifiers are given in note (a) of Table 3.

H I content with actual AGES-determined H I content. To do this, a catalogue of A 1367's brightest spiral members was compiled, with the following criteria. We initially selected late-type galaxies with an SDSS g -band magnitude < 15.5 within the sampled volume, i.e. 1 deg^2 surrounding the NW subcluster core in the velocity range $4000\text{--}9000 \text{ km s}^{-1}$ (approximately six times the velocity dispersion of the cluster). Only those objects with an optical disc diameter $> 0.37 \text{ arcsec}$ from GOLDMine (Gavazzi et al. 2003b) or, if unavailable, from the NED were selected. For the selected late-type galaxies, we determined their H I deficiency by comparing expected and observed H I content using the method of Haynes & Giovanelli (1984). Hubble type was taken from GOLDMine or, if unavailable, from NED. We selected all galaxies with Hubble type later than S0. The only exception, CGCG 097-125, an S0a, was included because of its unusually large H I mass.

Applying these criteria, we found the 26 bright late-type galaxies listed in Table 3 which gives details of their SDSS g -band magnitude

and $g - i$ colour, optical diameter from GOLDMine/NED, H I mass based on AGES flux, H I deficiency (or lower limit for AGES non-detections) based on AGES flux calculated using the method from Haynes & Giovanelli (1984) and parameters from Solanes et al. (1996), and separation parameters for galaxies with a close companion. A $g - i$ colour of 1.1 approximately coincides with the red-sequence threshold displayed in the colour–magnitude plot in fig. 12 of Cortese et al. (2008). For our sample, those galaxies with $g - i$ colour < 1.1 are referred to throughout the paper as *blue galaxies* and the rest referred to as *red galaxies*.

Fig. 14 shows the optical positions of the 26 spirals (red and blue symbols) and the positions of the 18 AGES H I detections (white circles). In the figure, the positions of the 16 selected galaxies with blue SDSS $g - i$ colours are indicated with blue symbols and the 10 with red SDSS $g - i$ colours with red symbols. Fig. 14 also indicates the distribution of ICM gas in the cluster based on ROSAT X-ray observations (black contours).

A shift in position in Fig. 14 between an AGES H I detection (white circle) relative to its respective optical position (red and blue symbols) is an indication of a real displacement when the offset exceeds 18 arcsec (7 kpc), the uncertainty in the AGES positions. This is only the case for CGCG 097-087 and CGCG 127-032. However, the much higher pointing accuracy of the VLA, ~ 4 arcsec (1.6 kpc), reveals that CGCG 097-062, CGCG 097-068, CGCG 097-072, CGCG 097-073, CGCG 097-079, CGCG 097-087 and CGCG 097-125 all have H I intensity maxima offsets relative to their optical counterparts larger than 3σ . In all the cases, the offset direction is consistent with that from the higher uncertainty AGES data. The projected magnitude and direction of the VLA offsets given in Table 2 are consistent with that expected for spirals on radial orbits experiencing ram pressure stripping, except CGCG 097-062, CGCG 097-068, CGCG 097-072 where the offset direction is not radially with respect to the cluster centre.

The four AGES detections in Fig. 14 without a selected late-type galaxy counterpart are the S0 galaxy CGCG 127-032, the two dwarfs, [GP82] 1227 and [BO85] 079, and an AGES detection to the NE of CGCG 097-068. CGCG 097-119 was not detected in the AGES survey because of its proximity to 3C264 and is therefore not included in our analysis.

5 DISCUSSION

The projected distribution, colour, H I content and velocities of the selected spirals throughout the sampled volume on large and small scales provide information on the recent history of the cluster as well as clues to the mechanisms impacting the galaxies' ISM. In the following sections, we consider the global H I properties, the role of ram pressure stripping attributable to the NW subcluster ICM and the evolutionary state of the spirals.

5.1 Global H I properties

Considered on a scale of several megaparsecs the pattern of H I deficiencies projected in RA for Coma and A 1367 in fig. 2 of Gavazzi (1989) show striking differences. From their figure, it is clear that with few exceptions the Coma spirals across the central $\sim 5^\circ$ of cluster are significantly H I deficient (>0.3). In contrast for A 1367, the significantly H I deficient spirals are found in a more narrow range of projected RA ($\sim 1^\circ$) and even at its centre a majority of the spirals are not deficient (H I deficiencies <0.3).

Within our sampled volume for A 1367 (\sim central 1.5 Mpc), the bright spirals, irrespective of H I content, are found preferentially projected on to the northern half (Fig. 14), with the AGES detections (white circles in Fig. 14) highly concentrated in a band running roughly E–W between declinations of $19^\circ 55'$ to $20^\circ 15'$.

As an initial step to understand the global H I properties in the sampled volume, we plotted, in Fig. 15, the H I deficiency of all the selected late-type galaxies as a function of projected distance from the cluster centre, with lower limits for H I non-detections, and BIG members confused in the AGES beam. The plot shows that the mean H I deficiency of the selected galaxies is appreciably greater than in the field indicating that the cluster environment has impacted the ISM of a significant fraction of them. However, unlike Coma where a clear increase in H I deficiency is seen within a radius of ~ 1 Mpc of the core (Bravo-Alfaro et al. 2000), there is no obvious correlation between H I deficiency and projected proximity to the cluster core. It should be noted, though, that the two interacting major subclusters revealed by the X-ray observations (see Fig. 1) complicate the investigation of any correlation between the cluster's

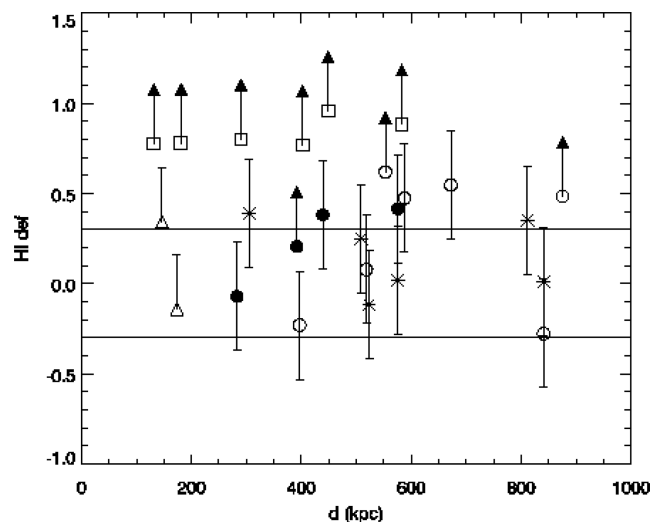


Figure 15. The H I deficiency of all the selected late-type galaxies in A 1367, (excluding CGCG 097-119) as a function of projected distance from the cluster centre. The following symbols are used to indicate the state (discussed in Section 5.3) of each spiral: A (asterisk), B (open circle), C (filled circle) and D (open square). For AGES non-detections the H I deficiency is a lower limit and is indicated with arrowheads. The two BIG spirals are confused in the AGES beam (triangles with upper error bar only) and in both cases the value is the lower limit for H I deficiency. The region between the horizontal lines approximates the natural range of variation expected in the field population.

ICM density and H I deficiency and in section 5.2 we try to address the effects which are specific to the NW subcluster.

5.2 Ram pressure stripping by the NW subcluster ICM

We are interested to know if the observed H I deficiencies can be explained in terms of ram pressure stripping. In order to quantify the role of this mechanism around the NW subcluster, we carried out a simple estimate of the strength of ram pressure as a function of radius from the NW subcluster ICM core. The ICM density (ρ_{ICM}) distribution was estimated using the hydrostatic isothermal β -model of Cavaliere & Fusco-Femiano (1976) with the gas profile parameters from Donnelly et al. (1998). Ram pressure values were derived from Gunn & Gott's (1972) equation: $P_{\text{ram}} = \rho_{\text{ICM}} \times v_{\text{rel}}^2$, where ρ_{ICM} is the density of the ICM at the galaxy position and v_{rel} is the galaxy's velocity relative to the ICM. We have no information about v_{rel} for the selected galaxies, although we consider a galaxy's radial velocity, relative to the cluster systemic velocity, as a lower limit for v_{rel} .

The results of this modelling of P_{ram} as a function of proximity to the NW core for four different values of v_{rel} , up to 2000 km s^{-1} (approximately the radial velocity difference of the BIG), are shown in Fig. 16. A spiral near the NW subcluster is expected to suffer ram pressure stripping if P_{ram} values exceed the restoring force of the galaxy's stellar and gas discs, at the gas disc's periphery, defined as $F_r = 2\pi G \sigma_{\text{stellar}} \sigma_{\text{gas}}$. The threshold ram pressure required to remove H I from the outer edge of the disc can be estimated from the typical value for the restoring force per unit area of $F_r = 2 \times 10^{-12} \text{ dyn cm}^{-2}$, obtained by Cayatte et al. (1994) for spiral galaxies in Virgo (dashed line in Fig. 16). The crossing time for the cluster is 1.7 Gyr (Boselli & Gavazzi 2006) making it likely that spirals within the central Mpc have been subject to ram pressure over periods of several times 10^8 yr . Modelling by

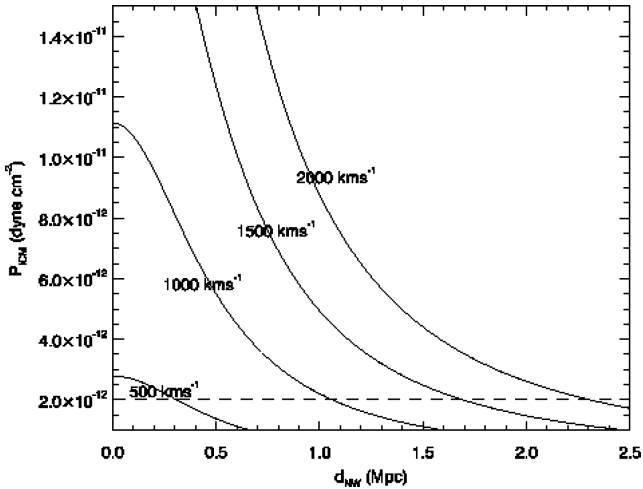


Figure 16. Ram pressure as a function of the distance from the X-ray emission maximum of the NW subcluster for v_{rel} of 500, 1000, 1500 and 2000 km s^{-1} . The dashed line indicates the threshold for ram pressure stripping based on Cayatte et al. (1994).

Roediger & Brügger (2007) indicates that for a mid-size spiral ($V_{\text{rot}} = 200 \text{ km s}^{-1}$) sustained exposure to ram pressures over periods of the order of 10^8 yr of $10^{-12} \text{ dyn cm}^{-2}$ will result in only minor stripping of H I, pressures of $10^{-11} \text{ dyn cm}^{-2}$ will cause significant stripping, while $10^{-10} \text{ dyn cm}^{-2}$ will almost completely remove the H I. Massive galaxies are expected to suffer proportionately less H I removal, and less massive galaxies proportionately more.

The implication of Fig. 16 and the Roediger & Brügger (2007) models is that any galaxy with $v_{\text{rel}} \geq 1000 \text{ km s}^{-1}$ anywhere within a radius of 1 Mpc of the NW subcluster will undergo weak-to-moderate ram pressure stripping. But, removal of large fractions of H I, i.e. $P_{\text{ram}} \geq 10^{-11} \text{ dyn cm}^{-2}$, would require a transit of the high-density ICM within $\sim 0.75 \text{ Mpc}$ of the cluster centre at a velocity in excess of 1500 km s^{-1} or transit within $\sim 0.25 \text{ Mpc}$ of the core at 1000 km s^{-1} .

To test the model predictions, we selected the 14 spirals from our sample which were potentially suffering ram pressure stripping solely attributable to the ICM of the NW subcluster. Virtually, all of these galaxies have radial velocities relative to the cluster of $\geq 500 \text{ km s}^{-1}$ and it seems reasonable to assume that most, if not all, are suffering ram pressure stripping of varying strengths given they are at projected radii of $\leq 0.8 \text{ Mpc}$. Fig. 17 shows a plot of H I deficiency against distance for these galaxies and, interestingly, only a modest increase in H I deficiency is seen when compared with the field. Furthermore, no correlation is seen with proximity to the NW subcluster ICM core. This observational result suggests that ram pressure stripping associated with the NW subcluster ICM core is relatively weak. The presence of undisturbed H I in CGCG 097-073's dwarf companion projected close to the NW-ICM core provides additional support to this statement.

Although the limited evidence for ram pressure stripping is broadly consistent with the expected ram pressure at the projected distances to the NW subcluster core (Fig. 16), the lack of correlation with radial distance from the core may imply that galaxies seen in projection to be located close to the core are in reality spread over a considerable distance. In the case of CGCG 097-068, a tidal interaction cannot be ruled out as an explanation of the observed H I characteristics.

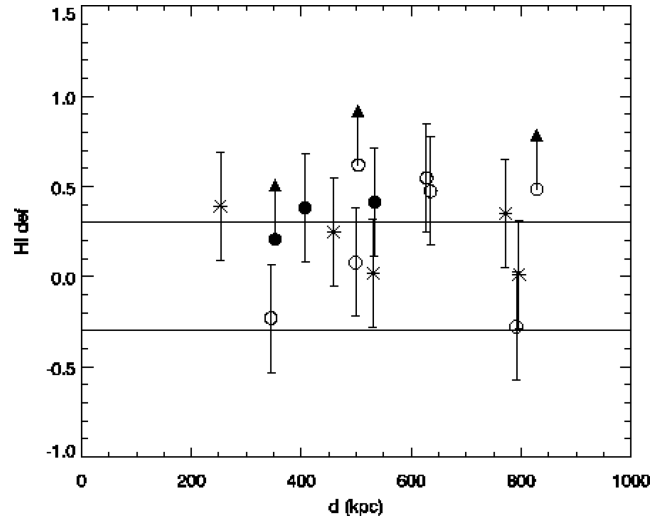


Figure 17. The H I deficiency of selected state A, B and C galaxies as a function of distance from the NW-ICM core. The following symbols are used to indicate the state (discussed in Section 5.3) of each spiral: A (asterisk), B (open circle) and C (filled circle). Galaxies with only upper error bars (arrowheads) are AGES non-detections so the value is the lower limit for H I deficiency. The region between the horizontal lines approximates the range expected in the field population.

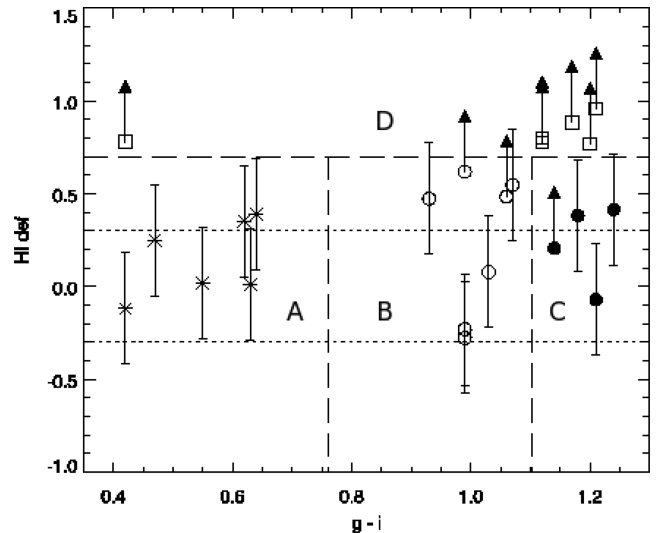


Figure 18. The H I deficiency of all the selected late-type galaxies (excluding CGCG 097-119 and BIG spirals) plotted against their SDSS $g - i$ colour. The long dashed lines mark the boundaries of the parameters defining the four evolutionary states marked A–D. The following symbols are used to indicate the state of each spiral: A (asterisk), B (open circle), C (filled circle) and D (open square). For AGES non-detections, the H I deficiency is a lower limit and is indicated with arrowheads. The region between the dotted horizontal lines approximates the natural range of variation expected in the field population.

5.3 Evolutionary states of the spirals

The colour and H I deficiency of a spiral are both properties indicative of its evolutionary state. In Fig. 18, we distinguish four broad evolutionary states (A–D). We classify the highly H I deficient galaxies (H I deficiency lower limit of ≥ 0.7) as state D spirals. The spirals with moderate or no H I deficiency (i.e. H I deficiency ≤ 0.7) are classified into three states (A, B and C) based on their

Table 4. Evolutionary states of spirals.

State	H I deficiency	SDSS colour $g - i$ (mag)	Plot symbol	number galaxies	median H I def	median $g - i$ colour (mag)
A	<0.7	<0.76	*	6	0.14	0.59
B	<0.7	$0.76 < \text{and} < 1.1$	○	7	0.47	0.99
C	<0.7	≥ 1.1	●	4	0.30	1.20
D	≥ 0.7	any	□	6	0.79	1.15

SDSS $g - i$ colour. C state spirals are red as defined in Section 4 (i.e. $g - i \geq 1.1$). The remaining blue spirals with moderate or no H I deficiency were classified as state A if their SDSS $g - i$ colour was <0.76 [the colour of the bluest type of late-type field spirals from Durbala et al. (2008), their table 3] and state B for those with $0.76 \leq g - i < 1.1$. Table 4 summarizes the parameters used to determine the evolutionary state of each spiral and the symbols used for them throughout the paper. The evolutionary state determined for each spiral is shown for convenience in the final column of Table 3. CGCG 097-125 and CGCG 097-114 have been excluded from the analysis because their evolution is likely to have been dominated by membership of the BIG compact group rather than the cluster.

While the choice of boundaries of our states could be debated, it is clear that the cluster contains spirals at significantly different stages of evolution, with the spirals in each state appearing to have reached a broadly similar evolutionary stage, probably as a result of sharing or passing through a common environment.

The discussion below is focused on the more evolved State C and D spirals where the impacts of the cluster environment are more pronounced. In contrast, spirals with less evolved states A and B are probably at earlier stages of their interactions and consequently show milder impacts, although a key question remains to be addressed, i.e. the mechanism(s) triggering the starbursts (state A).

The H I deficiencies of AGES detected state C spirals are modest compared to lower limits for the state D spirals, suggesting that they have not passed through the cluster's highest density ICM. The state C spirals include two of the three potentially interacting pairs, where the companion is projected within 2 arcmin (~ 50 kpc) and has a velocity within 500 km s^{-1} , and both galaxies are ≥ 0.5 arcmin (~ 12 kpc) in diameter (Table 3). The perturbation parameters, p_{gg} , for the state C pairs are ~ 8.7 (CGCG 097-102) and ~ 1.8 (CGCG 097-111) significantly above the value where the ISM is expected to be impacted. The interaction time-scales for the pairs is of the order of 10^8 years, in agreement with the value from Boselli & Gavazzi (2006). It is important to note that H I emission from close pairs could potentially be confused within Arecibo's ~ 3.5 arcmin beam underestimating the H I deficiency (AGES) for each member of the pair. But, in both the cases the spiral's companion is an early type making it unlikely the companion's H I makes a significant contribution. Moreover, three state C spirals (CGCG 097-102, CGCG 097-111 and CGCG 097-121) have optically disturbed morphologies in SDSS i -band images consistent with gravitational interactions. Signs of optical disturbance are also observed in three adjacent state A spirals, CGCG 097-092-1, CGCG 097-138 and [BO85]074, showing that tidal interactions, if important, could be affecting spirals in more than one evolutionary state. The high rate of disturbance in the optical morphology in this region suggests the spirals are subject to strong interactions possi-

bly related to their location at the intersection of the NW subcluster and the filament oriented towards the Coma cluster.

The state D spirals all have a red colour, except CGCG 097-093 which is exceptionally blue ($g - i = 0.42$) and has a disturbed stellar disc. The observed red colours and high H I deficiency are both expected results of a spiral making a transit through a high-density ICM core. An example of this is found in Virgo, i.e. the galaxy NGC 4568 (Boselli & Gavazzi 2006). The calculations for the NW subcluster (section 5.2) suggests that a core transit would be required to cause the H I deficiencies observed in the state D spirals under the ram pressure stripping scenario, although the ICM core transited may have been the SE subcluster. The tendency for the state D spirals further from the cluster centre to be redder and have higher velocities may be indicating that these spirals are a population of *backsplash* galaxies (Ellingson 2004), which were ram pressure stripped as they passed through the SE subcluster ICM core with a significant velocity component directed to the west.

6 CONCLUDING REMARKS

We have presented medium-resolution VLA data for a field located to the NW of A 1367's centre, and some higher resolution, but less sensitive, VLA data for a field containing the BIG. By using a catalogue of the brightest late-type members of the cluster, combining AGES and SDSS data, we have identified four evolutionary states with shared characteristics in terms of their combination of H I content and colour.

The overall picture from the H I deficiencies as a function of radial distance and calculations of ram pressure for the NW cluster (section 5.2) are both consistent with moderate levels of ram pressure stripping. However, the presence of spirals with a range of evolutionary states in projected and velocity space, particularly the spirals with more advanced evolutionary states (state C and D spirals), suggests an evolutionary process or processes operating on relatively local scales.

Consideration of the membership of the evolutionary states and individual spirals presents mixed, and sometimes contradictory, indicators of varying reliability for the dominant ISM removal process(es). The lack of correlation between H I deficiency and proximity to the NW subcluster core for the spirals likely to be affected by it, the presence of starbursts, the presence of galaxies with H I offset directions inconsistent with ram pressure, together with the elevated number of morphologically disturbed red and moderately H I deficient spirals (state C) possibly linked to interactions during infall, all suggest tidal effects. On the other hand, the presence of the highly H I deficient (state D) spirals and the possible case of gas falling back into the galaxy's potential following an ISM core transit (CGCG 097-072) support the ram pressure stripping model.

While the analysis above hints that different ISM removal mechanisms may be active in this cluster further observations are required

to discriminate between the hydrodynamic and tidal mechanisms. If anything, this paper shows that the picture in Abell 1367 is somewhat confusing, probably the result of it being less evolved than Coma and Virgo.

ACKNOWLEDGMENTS

We thank the referee for comments to an earlier version of the manuscript which have led to a much improved presentation.

HBA thanks CONACyT for grant No. 50794, the Royal Astronomical Society and the Academia Mexicana de Ciencias for financial support to carry out this work. CAC acknowledges the University of Guanajuato (DINPO) for grant 0131/07. MJH thanks the Royal Society for a Research Fellowship.

This research has made use of the NED which is operated by the Jet Propulsion Laboratory, California Institute of Technology, under contract with the National Aeronautics and Space Administration.

This research has made use of the SDSS. Funding for the SDSS and SDSS-II has been provided by the Alfred P. Sloan Foundation, the participating institutions, the National Science Foundation, the US Department of Energy, the National Aeronautics and Space Administration, the Japanese Monbukagakusho, the Max Planck Society and the Higher Education Funding Council for England. The SDSS web site is <http://www.sdss.org/>.

This work is partly based on observations obtained with *XMM-Newton*, an ESA science mission with instruments and contributions directly funded by ESA member states and the USA (NASA).

REFERENCES

- Amram P., Gavazzi G., Marcelin M., Boselli A., Vílchez J. M., Iglesias-Paramo J., Tarengi M., 2002, *Ap&SS*, 281, 401
- Auld R. et al., 2006, *MNRAS*, 371, 1617
- Baldwin J. A., Phillips M. M., Terlevich R., 1981, *PASP*, 93, 5
- Bekki K., 1999, *ApJ*, 510, L15
- Bekki K., Couch W. J., Shioya Y., 2002, *ApJ*, 577, 651
- Berrier J. C., Stewart K. R., Bullock J. S., Purcell C. W., Barton E. J., Wechsler R. H., 2009, *ApJ*, 690, 1292
- Bicker J., Fritze-v. Alvensleben U., Fricke K. J., 2002, *A&A*, 387, 412
- Blumenthal G. R., Faber S. M., Primack J. R., Rees M. J., 1984, *Nat*, 311, 517
- Boselli A. et al., 2005, *ApJ*, 623, L13
- Boselli A., Gavazzi G., 2006, *PASP*, 118, 517
- Boselli A., Gavazzi G., Combes F., Lequeux J., Casoli F., 1994, *A&A*, 285, 69
- Boselli A., Boissier S., Cortese L., Gil de Paz A., Seibert M., Madore B. F., Buat V., Martin D. C., 2006, *ApJ*, 651, 811
- Bravo-Alfaro H., Cayatte V., van Gorkom J. H., Balkowski C., 2000, *AJ*, 119, 580
- Bravo-Alfaro H., Cayatte V., van Gorkom J. H., Balkowski C., 2001, *A&A*, 379, 347
- Briggs D. S., 1995, *BAAS*, 27, 1444
- Butcher H. R., Oemler A., Jr, 1985, *ApJS*, 57, 665
- Byrd G., Valtonen M., 1990, *ApJ*, 350, 89
- Cavaliere A., Fusco-Femiano R., 1976, *A&A*, 49, 137
- Cayatte V., Kotanyi C., Balkowski C., van Gorkom J. H., 1994, *AJ*, 107, 1003
- Chincarini G. L., Giovanelli R., Haynes M., Fontanelli P., 1983, *ApJ*, 267, 511
- Chung A., van Gorkom J. H., Kenney J. D. P., Vollmer B., 2007, *ApJ*, 659, L115
- Chyży K. T., 2008, *A&A*, 482, 755
- Cortese L., Gavazzi G., Boselli A., Iglesias-Paramo J., Carrasco L., 2004, *A&A*, 425, 429
- Cortese L., Gavazzi G., Boselli A., Franzetti P., Kennicutt R. C., O'Neil K., Sakai S., 2006, *A&A*, 453, 847
- Cortese L. et al., 2008, *MNRAS*, 383, 1519
- Cowie L. L., Songaila A., 1977, *Nat*, 266, 501
- Dickey J. M., Gavazzi G., 1991, *ApJ*, 373, 347
- Donnelly R. H., Markevitch M., Forman W., Jones C., David L. P., Churazov E., Gilfanov M., 1998, *ApJ*, 500, 138
- Dressler A., 1980, *ApJ*, 236, 351
- Dressler A., 2004, in Mulchaey J. S., Dressler A., Oemler A., eds, *Clusters of Galaxies: Probes of Cosmological Structure and Galaxy Evolution*. Cambridge Univ. Press, Cambridge, p. 206
- Dressler A., Smail I., Poggianti B. M., Butcher H., Couch W. J., Ellis R. S., Oemler A. J., 1999, *ApJS*, 122, 51
- Durbala A., Sulentic J. W., Buta R., Verdes-Montenegro L., 2008, *MNRAS*, 390, 881
- Ellingson E., 2004, in Diaferio A., ed., *IAU Colloq. 195, Outskirts of Galaxy Clusters: Intense Life in the Suburbs*. Cambridge Univ. Press, Cambridge, p. 327
- Fasano G., Poggianti B. M., Couch W. J., Bettoni D., Kjærgaard P., Moles M., 2000, *ApJ*, 542, 673
- Fujita Y., Goto T., 2004, *PASJ*, 56, 621
- Fujita Y., Nagashima M., 1999, *ApJ*, 516, 619
- Gavazzi G., 1989, *ApJ*, 346, 59
- Gavazzi G., Boselli A., 1999, *A&A*, 343, 93
- Gavazzi G., Jaffe W., 1987, *A&A*, 186, L1
- Gavazzi G., Tarengi M., Jaffe W., Bokserberg A., Butcher H., 1984, *A&A*, 137, 235
- Gavazzi G., Contursi A., Carrasco L., Boselli A., Kennicutt R., Scodreggio M., Jaffe W., 1995, *A&A*, 304, 325
- Gavazzi G., Marcelin M., Boselli A., Amram P., Vílchez J. M., Iglesias-Paramo J., Tarengi M., 2001a, *A&A*, 377, 745
- Gavazzi G., Boselli A., Mayer L., Iglesias-Paramo J., Vílchez J. M., Carrasco L., 2001b, *ApJ*, 563, L23
- Gavazzi G., Cortese L., Boselli A., Iglesias-Paramo J., Vílchez J. M., Carrasco L., 2003a, *ApJ*, 597, 210
- Gavazzi G., Boselli A., Donati A., Franzetti P., Scodreggio M., 2003b, *A&A*, 400, 451
- Giovanelli R., Haynes M. P., 1985, *ApJ*, 292, 404
- Gunn J. E., Gott J. R. I., 1972, *ApJ*, 176, 1
- Haynes M. P., Giovanelli R., 1984, *AJ*, 89, 758
- Hota A., Saikia D. J., 2007, *Bull. Astr. Soc. India*, 35, 121
- Iglesias-Paramo J., Boselli A., Gavazzi G., Zaccardo A., 2004, *A&A*, 421, 887
- Kenney J. D. P., van Gorkom J. H., Vollmer B., 2004, *AJ*, 127, 3361
- Kronberger T., Kapferer W., Ferrari C., Unterguggenberger S., Schindler S., 2008, *A&A*, 481, 337
- Martig M., Bornaud F., 2008, *MNRAS*, 385, L38
- Mihos J. C., 2004, in Mulchaey J. S., Dressler A., Oemler A., eds, *Clusters of Galaxies: Probes of Cosmological Structure and Galaxy Evolution*. Cambridge Univ. Press, Cambridge, p. 277
- Moore B., Katz N., Lake G., Dressler A., Oemler A., 1996, *Nat*, 379, 613
- Moore B., Lake G., Quinn T., Stadel J., 1999, *MNRAS*, 304, 465
- Moran S. M., Ellis R. S., Treu T., Smith G. P., Rich R. M., Smail I., 2007, *ApJ*, 671, 1503
- Moss C., 2006, *MNRAS*, 373, 167
- Natarajan P., Kneib J.-P., Smail I., 2002, *ApJ*, 580, L11
- Nulsen P. E. J., 1982, *MNRAS*, 198, 1007
- Oemler A. J., 1974, *ApJ*, 194, 1
- Oemler A. J., Dressler A., Butcher H. R., 1997, *ApJ*, 474, 561
- Poggianti B. M. et al., 2009, *ApJ*, 697, 137
- Poggianti B. M., Smail I., Dressler A., Couch W. J., Barger A. J., Butcher H., Ellis R. S., Oemler A. J., 1999, *ApJ*, 518, 576
- Roediger E., Brügggen M., 2007, *MNRAS*, p. 765
- Sakai S., Kennicutt R. C. Jr, van der Hulst J. M., Moss C., 2002, *ApJ*, 578, 842
- Schneider S. E., Thuan T. X., Magri C., Wadiak J. E., 1990, *ApJS*, 72, 245
- Solanes J. M., Giovanelli R., Haynes M. P., 1996, *ApJ*, 461, 609

- Solanes J. M., Manrique A., García-Gómez C., González-Casado G., Giovanelli R., Haynes M. P., 2001, *ApJ*, 548, 97
- Springel V., White S. D. M., Tormen G., Kauffmann G., 2001, *MNRAS*, 328, 726
- Springob C. M., Haynes M. P., Giovanelli R., 2005, *ApJ*, 621, 215
- Sun M., Murray S. S., 2002, *ApJ*, 577, 139
- Sun M., Vikhlinin A., 2005, *ApJ*, 621, 718
- Tonnesen S., 2007, *New Astron. Rev.*, 51, 80
- van Gorkom J. H., 2004, in Mulchaey J. S., Dressler A., Oemler A., eds, *Clusters of Galaxies: Probes of Cosmological Structure and Galaxy Evolution*. Cambridge Univ. Press, Cambridge, p. 305
- Vollmer B., 2003, *A&A*, 398, 525
- Vollmer B., Cayatte V., Balkowski C., Duschl W. J., 2001a, *ApJ*, 561, 708
- Vollmer B., Braine J., Balkowski C., Cayatte V., Duschl W. J., 2001b, *A&A*, 374, 824
- Vollmer B., Balkowski C., Cayatte V., van Driel W., Huchtmeier W., 2004, *A&A*, 419, 35
- Vollmer B., Braine J., Pappalardo C., Hily-Blant P., 2008, *A&A*, 491, 455
- West M. J., Blakeslee J. P., 2000, *ApJ*, 543, L27
- Wilman D. J., Oemler A., Mulchaey J. S., McGee S. L., Balogh M. L., Bower R. G., 2009, *ApJ*, 692, 298

APPENDIX A: BIG

The BIG is an interesting case of a compact group that has been suggested to be infalling towards the core of the SE subcluster with a relative velocity of ~ 2000 km s $^{-1}$ (Cortese et al. 2006). As well as the two principal galaxies CGCG 097-114 and CGCG 097-125, the BIG contains an extraordinarily high concentration of dwarf galaxies with high star formation rates and extragalactic H II regions (Sakai et al. 2002; Gavazzi et al. 2003a). Deep H α imaging has revealed extensive gas streamers interpreted as resulting from a strong tidal interaction between members of the group (Cortese et al. 2006). H I in the BIG has previously been imaged using the WSRT by Sakai et al. (2002).

Our observations have higher spatial resolution that clearly show the offset between the highest density H I and the optical galaxy (Fig. 12). Weak H I emission was detected by us at the position of a knot 15 arcsec (6 kpc) east of knot K2a, with peak H I emission at 8190 km s $^{-1}$ or ~ 70 km s $^{-1}$ greater than K2a's optical velocity (Fig. 12). However, we did not pick up the large continuous region of low-density H I extending west of CGCG 097-125 and running from below K2a north to DW2 seen with the WSRT (Sakai et al. 2002), which is probably due to our lower sensitivity. We were also unable to confirm in our robust 0 cube the H I to the west of the optical position of the irregular blue galaxy CGCG 097-114, observed with the WSRT, although weak emission was found after applying natural weighting. The weak detection of CGCG 097-114 implies a large H I deficiency which is confirmed by the Arecibo determined H I mass of $3 \times 10^8 M_{\odot}$ (Cortese et al. 2006).

Regarding the relative location of the BIG with respect to the cluster centre, this is still matter of debate (Sakai et al. 2002; Gavazzi et al. 2003a; Cortese et al. 2006). The calculation discussed in Section 5.2 indicates that, if the group is within ~ 0.5 Mpc from the cluster centre, we should expect evidence of strong ram pressure stripping. This, however, would seem to be contradicted by the presence of substantial amounts of extended H I in the velocity range from 8000 to 8500 km s $^{-1}$, suggesting that either the BIG lies in the background of A1367 or it has just started its infall into the cluster centre.

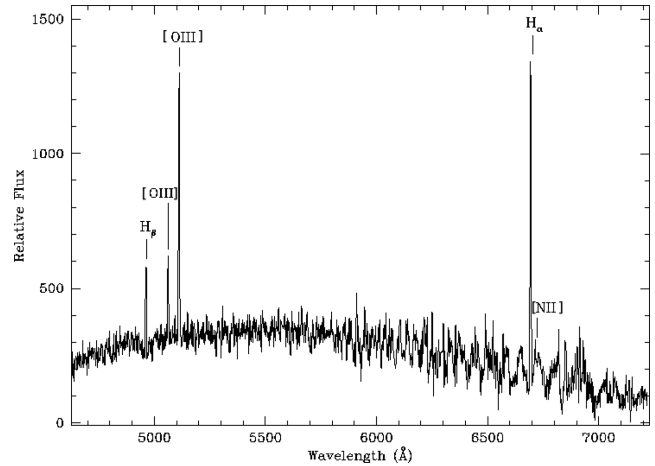


Figure B1. A 1367 [GP82]1227 emission line spectrum: SPM emission line spectrum showing H_{β} , [O III] (4958.9), [O III] (5006.8) [N II] (λ 6584) and H_{α} .

APPENDIX B: ABELL 1367[GP82]1227

We obtained a low-resolution (4.8 Å) spectrum of A 1367 [GP82]1227, covering the wavelength range 4630–7225 Å, in 2007 May (Fig. B1). The observation was carried out with the 2.12-m telescope at the San Pedro Mártir (SPM) Observatory in Mexico, using a Boller & Chivens spectrograph, a 600 l/mm grating and a 2K Thomson CCD. This configuration gave a dispersion of 1.3 Å pixel $^{-1}$. The slit was placed in an east–west direction passing through the central region of the galaxy. Four 20 min exposures were taken and the spectra were averaged after cosmic ray cleaning, extraction and wavelength calibration. A wavelength solution using about 30 He+Ar+Ne lamp lines gave an uncertainty of ~ 0.18 Å rms. Sky transparency was good, with the seeing slightly above 1 arcsec. Due to the faintness of the galaxy, the S/N obtained was only about 5 in the range 5500–6500 Å.

The spectrum of A 1367 [GP82]1227 shows the emission lines of H_{β} ($\lambda_{\text{rest}} = 4861.3$), [O III] (4958.9), [O III] (5006.8) and H_{α} (6562.8) at 4963.8, 5063.2, 5112.3 and 6700.4 Å, respectively. This gives an emission-line radial velocity of 6307 km s $^{-1}$, which is in good agreement with our H I velocity of 6239 km s $^{-1}$ (see Table 2). These emission lines indicate active star formation in A 1367 [GP82]1227. The [O III] (λ 5007)/ H_{β} and [N II] (λ 6584)/ H_{α} ratios are 2.64 and 0.03, respectively (note that [N II] is barely visible in the spectrum), putting this galaxy completely in the locus of star-forming galaxies in a BPT diagram (Baldwin, Phillips & Terlevich 1981). It was not possible to resolve the H α regions individually with the SPM 2.12 m.

APPENDIX C: CHANNEL MAPS OF THE VLA DETECTIONS

The channel maps for all VLA detections are available as supplementary online material (see the Supporting Information). Below as an example of the online material are the channel maps for CGCG 097-079.

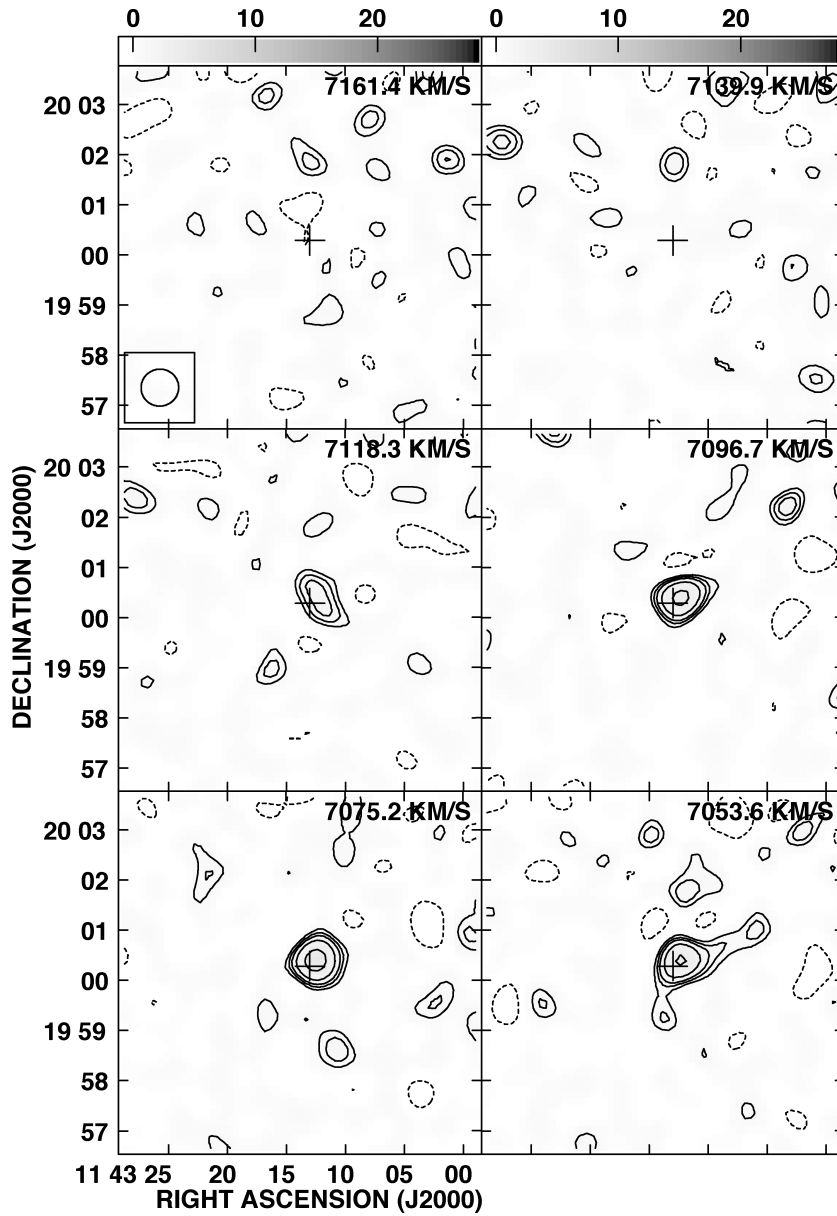


Figure C1. Channel maps for CGCG 097-079. The velocity in km s^{-1} is shown in the top-right corner of each frame. Contour levels are at -2σ , 2σ , 3σ , 4σ , 6σ , 10σ , 15σ , 20σ , 30σ and 45σ where σ corresponds to 0.36 mJy . The cross marks the centre of the optical galaxy.

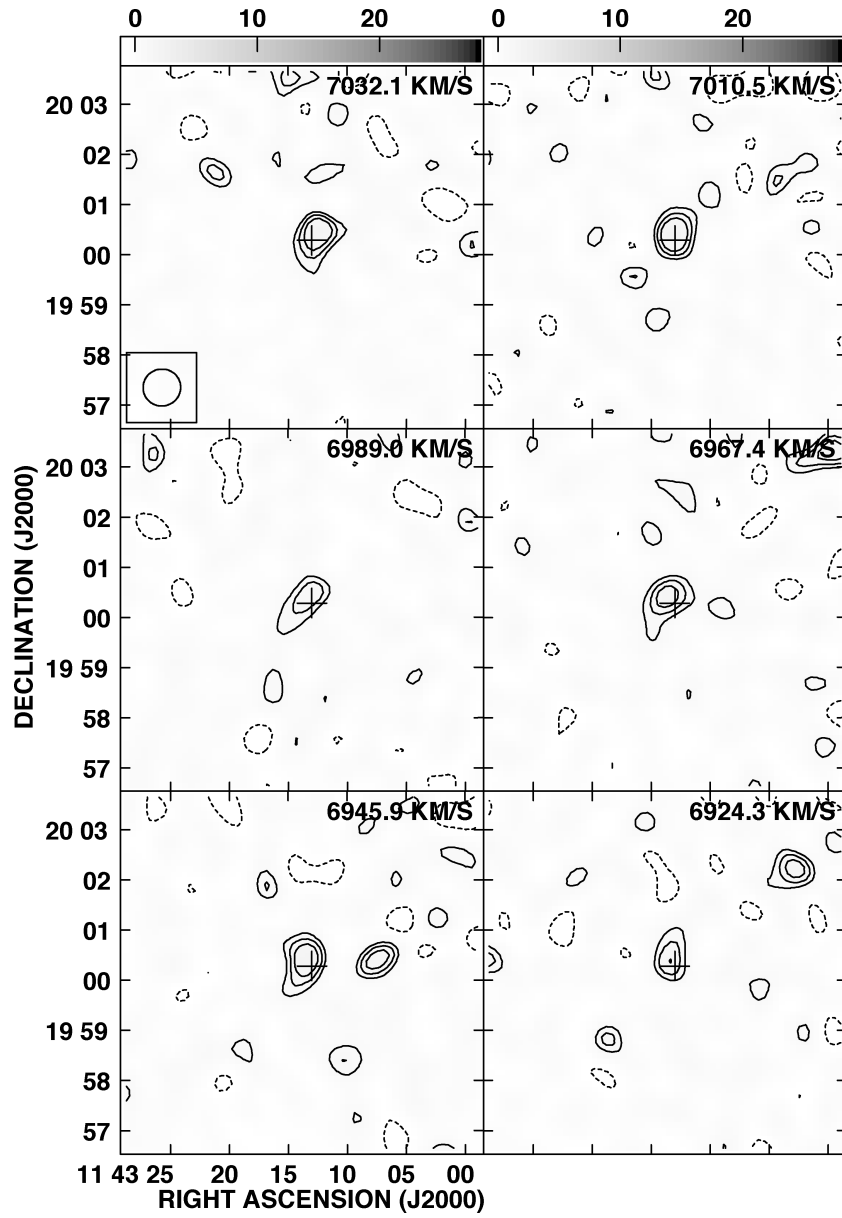
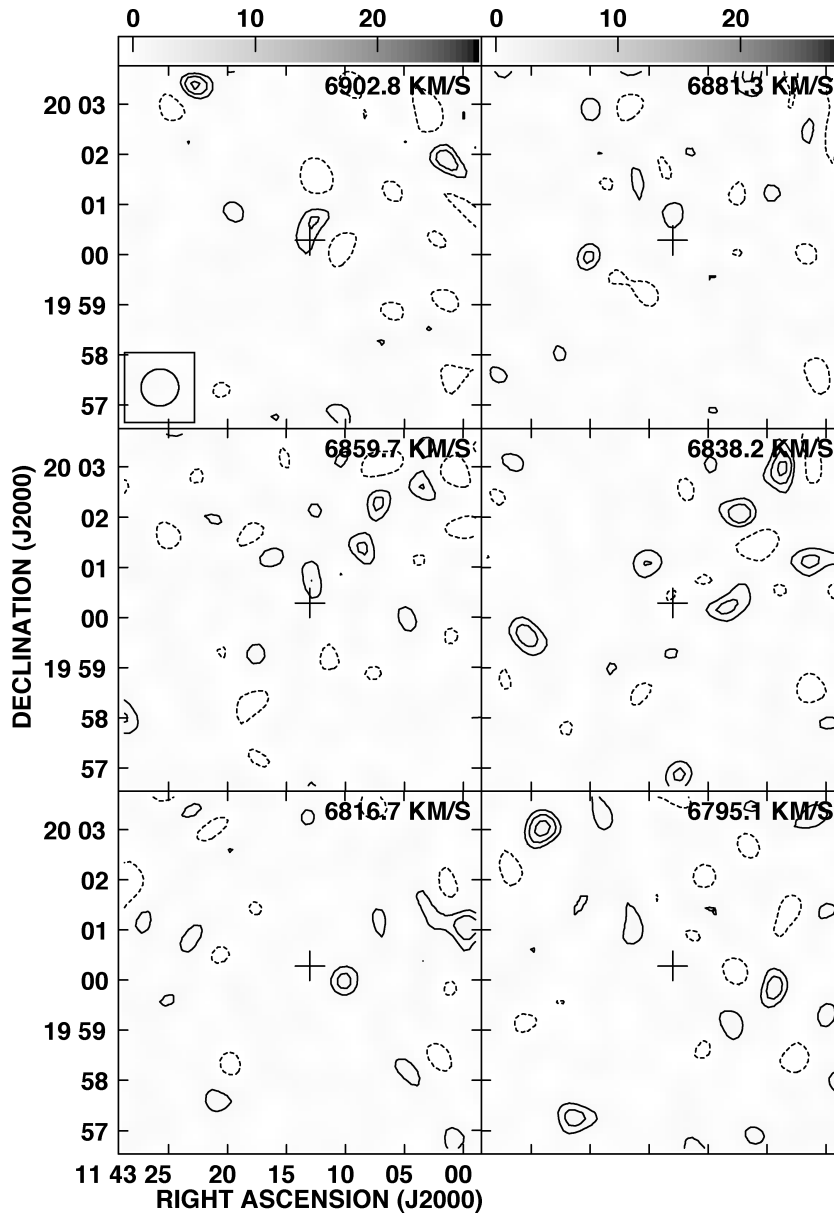


Figure C1 – continued

Figure C1 – *continued***SUPPORTING INFORMATION**

Additional Supporting Information may be found in the online version of this article:

Appendix C. Channel maps of the VLA detections.

Please note: Wiley-Blackwell are not responsible for the content or functionality of any supporting materials supplied by the authors.

Any queries (other than missing material) should be directed to the corresponding author for the article.

This paper has been typeset from a $\text{\TeX}/\text{\LaTeX}$ file prepared by the author.